Towards an Entropy Stable Spectral Element Framework for Computational Fluid Dynamics

Mark H. Carpenter,*
Comput. AeroSciences Branch (CASB) NASA LaRC, Hampton, VA 23681, USA,
Matteo Parsani,†
King Abdullah University of Science and Technology (KAUST),
Extreme Computing Research Center (ECRC),
Computer, Electrical and Mathematical Sciences & Engineering (CEMSE),
Thuwal, 23955-6900, Saudi Arabia ,
Travis C. Fisher,‡
Sandia National Laboratories, Albuquerque, NM 87123, USA,
Eric J. Nielsen §
CASB, NASA LaRC, Hampton, VA 23681, USA

Entropy stable (SS) discontinuous spectral collocation formulations of any order are developed for the compressible Navier-Stokes equations on hexahedral elements. Recent progress on two complementary efforts is presented. The first effort is a generalization of previous SS spectral collocation work to extend the applicable set of points from tensor product, Legendre-Gauss-Lobatto (LGL) to tensor product Legendre-Gauss (LG) points. The LG and LGL point formulations are compared on a series of test problems. Although being more costly to implement, it is shown that the LG operators are significantly more accurate on comparable grids. Both the LGL and LG operators are of comparable efficiency and robustness, as is demonstrated using test problems for which conventional FEM techniques suffer instability.

The second effort generalizes previous SS work to include the possibility of *p*-refinement at non-conforming interfaces. A generalization of existing entropy stability machinery is developed to accommodate the nuances of fully multi-dimensional summation-by-parts (SBP) operators. The entropy stability of the compressible Euler equations on non-conforming interfaces is demonstrated using the newly developed LG operators and multi-dimensional interface interpolation operators.

I. Introduction

Numerous strategies exist for constructing high-order discontinuous Galerkin (DG) spectral element methods. Popular variants adopt either the weak (integral) or strong (differential) form of the governing equations derived by integrating the equations once or twice against a test function. Various interior and interface flux approximations are used (e.g., quadrature free fluxes,[1] skew-symmetric[2]), as are various quadrature rules (e.g., Legendre-Gauss (LG)[a], Gauss-Lobatto, or Gauss-Radau points).

Each design choice is motivated by specific goals the practitioner deems desirable, such as efficiency, accuracy or flexibility. For example, Hesthaven and Warburton[3] twice integrate the equations by parts, thereby allowing the

*Corresponding author. mark.h.carpenter@nasa.gov.
†matteo.parsani@kaust.edu.sa
‡tcfishe@sandia.gov
§eric.j.nielsen@nasa.gov
[a]These points are also referred to as Gauss points.

boundary and interface conditions to be treated using the well established penalty approach. Gassner[2] uses a skew-symmetric split form of the equations to achieve telescoping convective terms in the compressible kinetic energy equation. Kopriva and Gassner[4] reported a survey of some common choices used when constructing DG algorithms, as well as their advantages and disadvantages.

An alternate design strategy based on a summation-by-parts (SBP), simultaneous-approximation-term framework (i.e., SBP-SAT operators), is used in references[5,6] to construct discontinuous high-order accurate collocation spectral element methods of any order. Therein, the primary motivation driving the design process is a semi-discrete operator that supports a nonlinear stability proof (entropy stability) for the three-dimensional (3D) compressible Navier-Stokes equations, on curvilinear hexahedral elements. The governing equations are discretized in strong form and adjoining elements are coupled using an SAT penalty approach technique.[7] The resulting algorithm is similar to the strong form nodal DG method reported in reference,[3] although differs in the treatment of the nonlinear Euler fluxes. A novel choice of nonlinear fluxes ensures conservation of mass, momentum and energy as well as the entropy within each element; hence element-wise entropy conservation. Entropy conservative/dissipative interface fluxes then guarantee boundedness of the entropy throughout the entire domain.[5,6] These numerical methods are referred to as entropy stable discontinuous collocation (SSDC) algorithms.

The SSDC algorithm are remarkably robust in the presence of shocks,[5,7] and is fully consistent with the Lax-Wendroff theorem[8] for weak solutions. The robustness is achieved because the semi-discrete thermodynamic entropy is provably bounded for all time in the L^2 norm, provided that density and temperature remain positive and boundary data is well-posed and preserves the entropy estimate of the interior operator. The nonlinear stability proof is extremely sharp; indeed entropy conservative interface fluxes guarantee global entropy conservation (neutrally stable). This sharpness is possible because stability is achieved without adding hyper-viscosity dissipation, de-aliasing or filtering the fluxes/solution. Assumptions of integral exactness are unnecessary to justify the proof (commonly used in weak form finite element methods (FEM)), because strong conservation form derivatives are approximated, rather than weak form integrals. Thus, over-integration of the nonlinear fluxes is unnecessary to more closely approximate integral exactness.

Although the formulations presented in references[5,6] are a huge step towards an operational entropy stable FEM framework, noteworthy challenges still remain: 1) arbitrary collocation points, 2) spatial- (h) and order- (p) adaptive refinement of hexahedral elements, and 3) use of triangle, prisms and tetrahedral elements.

Herein, an overview of two recent research efforts is reported towards an operational entropy stable discontinuous FEM framework of any order. First, an SBP-SAT framework is used to develop a generalized entropy stable spectral element formulation that includes a broader selection of collocation points. Next, p-refinement at a non-conforming interface is considered, and an entropy stable non-conforming coupling is constructed.

In the first effort, the entropy stable mechanics are extended to include solutions collocated at the Legendre-Gauss (LG) points (i.e., staggered SSDC algorithms), in contrast to the DG algorithm reported in[5,6] where the solution variables are all collocated at the 3D tensor product Legendre-Gauss-Lobatto (LGL) points. The studies reported here are motivated by the following observations.

First, it is well known that the integral exactness of the LG points exceeds that of the LGL points: $2p+1$ vs. $2p-1$. This advantage is consistent with the conclusions reported elsewhere[4] that indicate that the LG points have superior accuracy properties under many circumstances. The LG points are interior to element faces. Thus, solution data is *NOT* collocated on the element faces and as a consequence collocation points in adjacent elements are not duplicated on the interfaces. An added benefit is that variables are not collocated at the corners of the element. Thus, geometric boundary discontinuities are handled in an integral sense without explicit knowledge of the boundary singularity.

A second compelling motivation for the LG points is to facilitate data movement on non-conforming interfaces. Storing the solution at the LG points naturally leads to interface penalties that are enforced on the projected LG point of each face. In addition to the superior accuracy properties of the LG points, preliminary derivations indicate vastly superior structural properties of the non-conforming element transfer operators.

The staggered grid component of this work is nearing completion and is documented in a recent NASA technical report[9] and in a submitted journal publication.[10] A brief summary of the important findings include the following. Extensive numerical tests of the new staggered SSDC operators demonstrate superior accuracy as compared with the LGL operators[5,6] of equivalent polynomial order on the same grid. They are, however, more costly to implement. Preliminary investigations indicate that the increased accuracy more than offsets the additional cost, particularly at low polynomial order. In particular, both cost and accuracy of the staggered algorithm for a solution polynomial order

p are comparable to those of the LGL operators[5,6] with a solution polynomial order of $p+1$. This finding can likely be generalized to the large family of high-order accurate discretizations which includes the linearly stable spectral difference[11,12] and flux reconstruction schemes.[13,14] The staggered operators are anticipated to be more advantageous for implicit temporal integrators because of work scaling arguments for the linear and nonlinear solvers.

The second effort, focuses on p-refinement at a non-conforming interface. Consider the problem of p-refinement between two adjoining elements of polynomial orders p and $p+1$, respectively. This scenario requires data movement from adjoining interfaces onto an common intermediate mortar; in general the quadrature points on either side of the interface do not coincide. Thus, the entropy stability proofs presented in references[5,6] do not immediately extend to this extremely important scenario. The solution to this problem relies on the ability to move data around the element while maintaining entropy stability. Indeed, it is closely related to the staggered-grid problem discussed previously.

The non-conforming interface component of this work is maturing, but is far from being fully operational. Entropy conservative/stable p-adaptive refinement mechanics have been developed for the nonlinear compressible Euler equations on hexahedral elements. This work required a significant generalization of the existing entropy stability mechanics to accommodate fully multi-dimensional summation-by-parts (SBP) operators. This generalized entropy machinery will facilitate the analysis of other element types, including the closely related scenario of h-refinement. Successful completion of these two objectives, brings the entropy stable spectral collocation framework closer to the maturity of conventional DG-FEM, but with the rigor of provably non-linearly stable semi-discrete operators.

The paper is organized as follows. Section II summarizes the theoretical aspects of SBP-SAT operators needed in this work, including a generalization to two-dimensional (2D) operators. Section III presents in a concise way the continuous entropy stability analysis of the compressible Navier-Stokes equations and the main results of entropy consistent and entropy stable SBP operators of any order. Section IV includes a novel entropy stability proof for the staggered-grid approach that focuses on one-dimensional (1D) Burgers' equation. In section V two choices of SBP operators for the 3D compressible Navier-Stokes equations on staggered grids are presented, namely the fully-staggered and the semi-staggered approaches. Section VI summarizes the entropy stable interface coupling used for conforming interfaces. Section VII extends the results presented in the previous section to the non-conforming case when different polynomial orders are used on the left and right side of the interface (i.e., p-refinement). Section VIII summarizes the results of the paper for both conforming and non-conforming interfaces and the entropy stable staggered algorithms. Conclusions are drawn in Section IX.

II. Theory: SBP-SAT Operators

II.A. Summation-by-parts Operators

II.A.1. One Spatial Dimension

First derivative operators that satisfy the summation-by-parts (SBP) convention, discretely mimic the integration-by-parts property

$$\int_{x^L}^{x^H} \phi \frac{\partial q}{\partial x}\,\mathrm{d}x = \phi\, q|_{x^L}^{x^H} - \int_{x^L}^{x^H} \frac{\partial \phi}{\partial x}\, q\,\mathrm{d}x, \tag{II.1}$$

with ϕ an arbitrary scalar test function. At the discrete level, this mimetic property is achieved by constructing the first derivative approximation, $\mathcal{D}\phi$, with an operator in the form

$$\begin{gathered} \mathcal{D} = \mathcal{P}^{-1} Q, \quad \mathcal{P} = \mathcal{P}^\top, \quad \zeta^\top \mathcal{P} \zeta > 0, \quad \zeta \neq \mathbf{0}, \\ Q^\top = \mathcal{B} - Q, \quad \mathcal{B} = \mathrm{Diag}\left(-1, 0, \ldots, 0, 1\right), \end{gathered} \tag{II.2}$$

where ζ is an arbitrary vector. The matrix $\mathcal{P}$ can be thought of as a mass matrix (or integrator) much like in the finite element framework, or a volume that contains local grid information in the context of finite volume or finite difference numerical methods. The nearly skew-symmetric matrix Q, is an undivided differencing operator; all rows sum to zero, as do all columns save the first and last, which sum to -1 and 1, respectively.

While the matrix $\mathcal{P}$ need not be diagonal, the class of diagonal norm SBP operators play a crucial roll in the development of entropy stable (SS) SBP simultaneous-approximation-term (SAT) operators (see references[15,5,6,16,17]).

Integration in the approximation space is conducted using an inner product with the integration weights contained in the norm $\mathcal{P}$,

$$\int_{x^L}^{x^H} \phi \frac{\partial q}{\partial x} \mathrm{d}x \approx \phi^\top \mathcal{P} \mathcal{D} \mathbf{q}, \tag{II.3}$$

where

$$\mathbf{q}(\mathbf{x}) = (q(x_1), q(x_2), \ldots, q(x_N))^\top, \quad \text{with} \quad \mathbf{x} = (x_1, \ldots, x_N), \quad x_1 = x^L, \quad x_N = x^H, \tag{II.4}$$

is the projection of continuous variables q onto the grid $\mathbf{x}$. Substituting equation (II.2) into equation (II.3), the mimetic SBP property is demonstrated,

$$\phi^\top \mathcal{P} \mathcal{P}^{-1} \mathcal{Q} \mathbf{q} = \phi^\top \left(\mathcal{B} - \mathcal{Q}^\top \right) \mathbf{q} = \phi_N q_N - \phi_1 q_1 - \phi^\top \mathcal{D}^\top \mathcal{P} \mathbf{q}. \tag{II.5}$$

II.A.2. Telescopic Flux Form

All 1D SBP derivative operators, $\mathcal{D}$, can be manipulated into the telescopic flux form,

$$f_x(\mathbf{q}) = \mathcal{P}^{-1} \mathcal{Q} \mathbf{f} + \mathcal{T}_{(p+1)} = \mathcal{P}^{-1} \Delta \bar{\mathbf{f}} + \mathcal{T}_{(p+1)}. \tag{II.6}$$

where the $N \times (N+1)$ matrix Δ is

$$\Delta = \begin{pmatrix} -1 & 1 & 0 & 0 & 0 & 0 \\ 0 & -1 & 1 & 0 & 0 & 0 \\ 0 & 0 & \ddots & \ddots & 0 & 0 \\ 0 & 0 & 0 & -1 & 1 & 0 \\ 0 & 0 & 0 & 0 & -1 & 1 \end{pmatrix}, \tag{II.7}$$

that calculates the undivided difference of the two adjacent fluxes. All conservative and accurate flux gradients may be constructed in the form of (II.6) for all 1D SBP operators, $\mathcal{Q}$, a fact that is reiterated in the following lemma presented without proof. (The original proof appears in reference[18]).

Lemma 1. *All differentiation matrices that satisfy the 1D SBP convention given in eq.* (II.2) *are telescoping operators in the norm* $\mathcal{P}$.

II.A.3. Two Spatial Dimensions

A definition of two-dimensional (2D) SBP operators that is sufficient for the non-conforming interface operators, is adapted from the more general definition proposed in reference.[19] The extension of the matrix operators proposed in equations (II.2), (II.3), and (II.5) proceeds as follows.

Consider a 2D set of points $\mathbf{X}_{xy} = [(x_i, y_i)]_{i=1}^N$ on a bounded domain $\Omega \subset \mathbb{R}^2$, with a piece-wise smooth boundary Γ. Define the 2D monomial basis functions

$$\mathcal{S}_{mn} = x^m y^n, \quad 0 \leq m+n \leq p \tag{II.8}$$

and their projection onto the grid $\mathbf{X}_{xy}$ as

$$\mathcal{S}_{mn}(\mathbf{X}_{xy}) = (s_{mn}(x_1, y_1), \ldots, s_{mn}(x_N, y_N))^\top, \quad \mathcal{S}'_{mn}(\mathbf{X}_{xy}) = \left(s'_{mn}(x_1, y_1), \ldots, s'_{mn}(x_N, y_N)\right)^\top, \tag{II.9}$$

where the symbol $(\cdot)'$ denotes the derivative with respect to the independent variables x (respectively y). A two-dimensional SBP derivative operator $\mathcal{D}_x$ (i.e., x-direction) satisfies the following accuracy and structural constraints.

Definition 1. *The matrix* $\mathcal{D}_x$ *is an SBP approximation of* $\frac{\partial}{\partial x}$ *on the points* $\mathbf{X}_{xy}$ *if it satisfies the following conditions.*

- $\mathcal{D}_x = \mathcal{P}^{-1} \mathcal{Q}_x \quad , \quad \mathcal{Q}_x + \mathcal{Q}_x = \mathcal{B}_x \quad , \quad \mathcal{P} = \mathcal{P}^T \ , \quad \zeta^\top \mathcal{P} \zeta > 0 \, , \quad \zeta \neq \mathbf{0},$

- $\mathcal{B}_x = \mathcal{B}_x{}^T$ *and* $\mathcal{S}_{mnk}{}^T \mathcal{B}_x \mathcal{S}_{mn\ell} = \oint_\Gamma \mathcal{S}_{mnk} \mathcal{S}_{mn\ell} \vec{n}_x \, d\Gamma$,
- $\mathcal{D}_x \mathcal{S}_{mn} = \mathcal{S}'_{mn}$, $0 \le m+n \le p$ *or equivalently* $\sum_{\ell=1}^{N} q_{\ell k} x_k^m y_k^n = \mathcal{P}_{(i)(i)} \, m x_i^{m-1} y_i^n$, $0 \le m+n \le p$,

with n_x *the outward facing normal on* Γ*, and* $\mathcal{S}_{mnk}$ *and* $\mathcal{S}_{mn\ell}$ *are taken from the admissible set of monomial polynomials defined in equation* (II.8).

Note that definition 1 naturally accounts for tensor product extensions of the one dimensional operators (i.e., $\mathcal{D}_x = \mathcal{D}_{x_1} \otimes I_{x_2}$), but also allows for non-tensor formulations via the expanded definition of the boundary operators, $\mathcal{B}_x$. Multi-dimensional polynomials (or general smooth functions $F(U(x,y))$ that are of order greater than p are differentiated to design order by $\mathcal{D}_x$:

$$\mathcal{D}_x F(U(x,y)) = \frac{\partial F}{\partial U}\frac{\partial U}{\partial x} + O\left((\delta x)^p\right). \tag{II.10}$$

II.B. Spectral Collocation Differentiation and Interpolation Operators

II.B.1. Differentiation

Consider the SBP operators constructed at the LGL points,[20] which include the end points of the interval, x^L and x^H. The complete discretization operator for the fourth-order accurate polynomial interpolation ($p = 4$) in the standard one-dimensional (1D) element ($x^L = -1$, $x^H = +1$) is illustrated in Figure 1. In this figure, the solution points are identified with $\bullet$ and the flux points are identified with $|$. The latter points are similar in nature to the control volume edges employed in the finite volume method and are used to prove the nonlinear stability (entropy stability) as briefly shown in Section III.C, (see references[5,6] for a more detailed discussion).

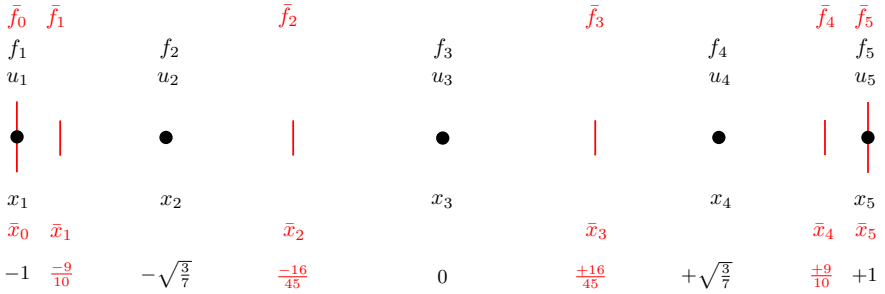

Figure 1. The one-dimensional discretization for the fourth-order accurate polynomial interpolation ($p = 4$) LGL collocation is illustrated. Solution points are identified with $\bullet$ and the flux points are identified with $|$.

Define the Lagrange basis polynomials relative to the N discrete LGL points, $\mathbf{x}$, as

$$L_j(x) = \prod_{\substack{k=1 \\ k \neq j}}^{N} \frac{x - x_k}{x_j - x_k}, \qquad 1 \le j \le N. \tag{II.11}$$

Assume that a smooth and (infinitely) differentiable function $f(x)$ is defined on the interval $x^L = -1 \le x \le 1 = x^H$. Reading the function f and its derivative $\frac{df}{dx}$ at the discrete points, $\mathbf{x}$, yields the vectors

$$\begin{aligned} \mathbf{f}(\mathbf{x}) &= \left(f(x_1), f(x_2), \cdots, f(x_{N-1}), f(x_N)\right)^\top, \\ \mathbf{f}'(\mathbf{x}) &= \left(\frac{df}{dx}(x_1), \frac{df}{dx}(x_2), \cdots, \frac{df}{dx}(x_{N-1}), \frac{df}{dx}(x_N)\right)^\top. \end{aligned} \tag{II.12}$$

The interpolation polynomial $f_N(x)$ (of order $p = N-1$) that collocates $f(x)$ at the discrete points, $\mathbf{x}$, is given by the contraction

$$f(x) \approx f_N(x) = \mathbf{L}(x;\mathbf{x})^\top \mathbf{f}(\mathbf{x}), \tag{II.13}$$

where $\mathbf{L}(x;\mathbf{x})$ is a column vector whose components are the Lagrange basis polynomials relative to the nodes $\mathbf{x}$ (i.e., $L_j(x)$ in equation (II.11)). Note that the explicit dependence of $\mathbf{L}$ on the independent variable x and the set of point $\mathbf{x}$ is indicated for completeness.[b]

[b] f_N is a polynomial of order p in the independent variable x.

Theorem 2. *The derivative operator that exactly differentiates an arbitrary p-th order polynomial ($p = N-1$) at the collocation points,* $\mathbf{x}$*, is*

$$\mathcal{D} = (d_{ij}) = \left(\frac{dL_j}{dx}(x_i) \right), \tag{II.14}$$

where $\frac{dL_j}{dx}(x_i)$ denotes the derivatives of the L_j Lagrange basis polynomial with respect to x evaluated at the collocated node x_i. This element corresponds to the element in the j-th column and i-th row of the differentiation matrix $\mathcal{D}$.

Proof. The proof to this theorem can be found in reference 9. □

A representation of the differentiation operator $\mathcal{D}$, which satisfies all the requirements for being an SBP operator is given in the following theorem

Theorem 3. *The derivative operator that exactly differentiates an arbitrary p-th order polynomial ($p = N-1$) at the collocation points,* $\mathbf{x}$*, can be expressed as*

$$\mathcal{D} = \mathcal{P}^{-1} \mathcal{Q} \tag{II.15}$$

with

$$\mathcal{P} = \sum_\ell \mathbf{L}(\eta_l;\mathbf{x})\mathbf{L}(\eta_l;\mathbf{x})^\top \omega_\ell \quad , \quad \mathcal{Q} = \sum_\ell \mathbf{L}(\eta_l;\mathbf{x})\mathbf{L}'(\eta_l;\mathbf{x})^\top \omega_\ell, \tag{II.16}$$

where η_ℓ and ω_ℓ, $1 \le l \le N$, are the abscissae of the LGL points and their quadrature weights, respectively. $\mathbf{L}(x;\mathbf{x})$ *is a column vector whose components are the Lagrange basis polynomials relative to the discrete nodes* $\mathbf{x}$ *(i.e., $L_j(x)$ in equation (II.11))*

Proof. The proof to this theorem can be found in reference 9, Appendix B. □

The matrix $\mathcal{P}$ in (II.16) is symmetric and positive definite for any vector $\mathbf{x}$.[20] Furthermore, because the discrete points $\mathbf{x}$ are the LGL points, the matrix $\mathcal{P}$ is a diagonal approximation (i.e., the so-called "mass lumped" approximation) of the full $\hat{\mathcal{P}}$-norm, which is defined as $\hat{\mathcal{P}} = (p_{ij}) = \int_{-1}^{1} \mathbf{L}(x;\mathbf{x})\mathbf{L}(x;\mathbf{x})^\top$ (see Appendix B in[9]). To the best of our knowledge, diagonal norm SBP operators are necessary to prove strict entropy conservation or entropy stability.[21,22,9]

II.B.2. Interpolation From and To Legendre-Gauss and Legendre-Gauss-Lobatto Points

Define on the interval $-1 \le x \le 1$, the vectors of discrete point,

$$\begin{aligned} \tilde{\mathbf{x}} &= (\widetilde{x}_1, \widetilde{x}_2, \cdots, \widetilde{x}_{M-1}, \widetilde{x}_M)^\top, \quad -1 \le \widetilde{x}_1, \widetilde{x}_2, \cdots, \widetilde{x}_{M-1}, \widetilde{x}_M \le 1; \\ \mathbf{x} &= (x_1, x_2, \cdots, x_{N-1}, x_N)^\top, \quad -1 \le x_1, x_2, \cdots, x_{N-1}, x_N \le 1. \end{aligned} \tag{II.17}$$

Herein, the discrete points $\tilde{\mathbf{x}}$ and $\mathbf{x}$ are the LG points, and the LGL points, respectively. All the scalars, vectors, and matrices associated to the LG points are denoted with a "tilde" symbol. Next, define the interpolation operators that move data between $\tilde{\mathbf{x}}$ and $\mathbf{x}$:

$$\begin{aligned} I_{LGL2G} &= \tilde{\mathcal{P}}^{-1} \mathcal{R}_{LG-LGL}, \\ I_{G2LGL} &= \mathcal{P}^{-1} \mathcal{R}_{LG-LGL}^\top, \\ \tilde{\mathcal{P}}\, I_{LGL2G} &= I_{LG\to LGL}^\top \mathcal{P}, \end{aligned} \tag{II.18}$$

where

$$\mathcal{R}_{LG-LGL} = \int_{-1}^{1} \mathbf{L}(x;\tilde{\mathbf{x}})\, \mathbf{L}(x;\mathbf{x})^\top \, dx. \tag{II.19}$$

In reference,[9,10] it is shown that these polynomial interpolation operators exist and satisfy the relations (II.18), provided that the LGL points are of higher polynomial orders than the LG points (i.e., $N > M$).

II.B.3. Interpolation From and To Interior Legendre-Gauss and Interface Legendre-Gauss Points

In the case of non-conforming interface, the discrete points $\tilde{\mathbf{x}}$ and $\mathbf{x}$ are the interior LG points (i.e., the solution points) and the interface LG points (i.e., the interface flux points), respectively. The interpolation operators that move data between $\tilde{\mathbf{x}}$ and $\mathbf{x}$ are computed as in (II.18) and are defined as

$$\begin{aligned} I_{H2L} &= \tilde{\mathcal{P}}^{-1}\,\mathcal{R}_{L-H}, \\ I_{L2H} &= \mathcal{P}^{-1}\mathcal{R}_{L-H}^{\top}, \\ \tilde{\mathcal{P}}\,I_{H2L} &= I_{L\to H}^{\top}\,\mathcal{P}, \end{aligned} \tag{II.20}$$

where

$$\mathcal{R}_{L-H} = \int_{-1}^{1} \mathbf{L}(x;\tilde{\mathbf{x}})\,\mathbf{L}(x;\mathbf{x})^{\top}\,dx. \tag{II.21}$$

Note that the subscript L and H in (II.20) are used to denote the "low" and "high" polynomial order.

III. Entropy Consistent and Entropy Stable SBP Operators

III.A. Governing Equations

Consider the three-dimensional (3D) compressible Navier-Stokes equations for a calorically perfect gas expressed in the form

$$\begin{aligned} &\frac{\partial q}{\partial t} + \frac{\partial f_i}{\partial x_i} = \frac{\partial f_i^{(V)}}{\partial x_i}, \quad x \in \Omega, \quad t \in [0,\infty), \\ &Bq = g^{(B)}(x,t), \quad x \in \partial\Omega, \quad t \in [0,\infty), \\ &q(x,0) = g^{(0)}(x), \quad x \in \Omega, \end{aligned} \tag{III.1}$$

where the Cartesian coordinates, $x = (x_1, x_2, x_3)^{\top}$, and time, t, are independent variables, and index sums are implied. The vectors q, f_i, and $f_i^{(V)}$ are the conserved variables, and the conserved inviscid and viscous fluxes, respectively. Without loss of generality, a 3D box

$$\Omega = [x_1^L, x_1^H] \times [x_2^L, x_2^H] \times [x_3^L, x_3^H]$$

is chosen as our computational domain with $\partial\Omega$ representing the boundary of the domain. The boundary vector $g^{(B)}$ is assumed to contain linearly well-posed Dirichlet and/or Neumann data. Herein, we have omitted a detailed description of the 3D compressible Navier-Stokes equations because it can easily be found in literature.

III.B. Continuous Analysis

Consider the (nonlinear) compressible Navier-Stokes equations given in equation (III.1). This system of incomplete parabolic partial differential equations (PDEs) have a quadratic or otherwise convex extension of its original form, that when integrated over the physical domain, Ω, depends only on boundary data and dissipative terms. This convex extension yields the entropy function and provides a mechanism for proving the stability in the L^2 norm of the nonlinear system of PDEs (III.1). In fact, Dafermos[23] showed that if a system of conservation laws is endowed with a convex entropy function, $S = S(q)$, a bound on the global estimate of S can be converted into an a priori estimate on the solution vector q (e.g., the solution of system (III.1)).

Definition 2. *A scalar function $S = S(q)$ is an entropy function of system (III.1) if it satisfies the following conditions:*

- *Differentiation of the convex function $S(q)$, simultaneously contracts all the inviscid spatial fluxes as follows*

$$\frac{\partial S}{\partial q}\frac{\partial f_i}{\partial x_i} = \frac{\partial S}{\partial q}\frac{\partial f_i}{\partial q}\frac{\partial q}{\partial x_i} = \frac{\partial F_i}{\partial q}\frac{\partial q}{\partial x_i} = \frac{\partial F_i}{\partial x_i}, \quad i = 1,2,3. \tag{III.2}$$

  The components of the contracting vector, $\partial S/\partial q$, are the entropy variables denoted as $w^{\top} = \partial S/\partial q$. $F_i(q)$ are the entropy fluxes in the i-direction.

- *The entropy variables, w, symmetrize system* (III.1) *if w assumes the role of a new independent variable (i.e., $q = q(w)$). Expressing equations* (III.1) *in terms of w yields*

$$\frac{\partial q}{\partial t} + \frac{\partial f_i}{\partial x_i} - \frac{\partial f_i^{(V)}}{\partial x_i} = \frac{\partial q}{\partial w}\frac{\partial w}{\partial t} + \frac{\partial f_i}{\partial w}\frac{\partial w}{\partial x_i} - \frac{\partial}{\partial x_i}\left(\widehat{c}_{ij}\frac{\partial w}{\partial x_j}\right) = 0, \quad i = 1,2,3, \tag{III.3}$$

with the symmetry conditions: $\partial q/\partial w = (\partial q/\partial w)^\top$, $\partial f_i/\partial w = (\partial f_i/\partial w)^\top$ and $\widehat{c}_{ij} = \widehat{c}_{ij}^\top$.[c]

An extensive and detailed entropy analysis of the Euler and compressible Navier-Stokes equations can be found for instance, in references 25, 26, 5, 22, 6, 16, 27, and the references therein.

Contracting system (III.1) with the entropy variables, w, results in the differential form of the (scalar) entropy equation,

$$\begin{aligned}\frac{\partial S}{\partial q}\frac{\partial q}{\partial t} + \frac{\partial S}{\partial q}\frac{\partial f_i}{\partial x_i} = \frac{\partial S}{\partial t} + \frac{\partial F_i}{\partial x_i} = \frac{\partial S}{\partial q}\frac{\partial f_i^{(V)}}{\partial x_i} &= \frac{\partial}{\partial x_i}\left(w^\top f_i^{(V)}\right) - \left(\frac{\partial w}{\partial x_i}\right)^\top f_i^{(V)} \\ &= \frac{\partial}{\partial x_i}\left(w^\top f_i^{(V)}\right) - \left(\frac{\partial w}{\partial x_i}\right)^\top \widehat{c}_{ij}\frac{\partial w}{\partial x_j}.\end{aligned} \tag{III.4}$$

Integrating equation (III.4) over the domain yields a global conservation statement for the entropy in the domain

$$\frac{d}{dt}\int_\Omega S\,\mathrm{d}\mathbf{x} = \left[w^\top f_i^{(V)} - F_i\right]_{\partial\Omega} - \int_\Omega w_{x_i}^\top \hat{c}_{ij} w_{x_j}\,\mathrm{d}\mathbf{x}. \tag{III.5}$$

References[21,22] prove that the five-by-five matrices $\hat{c}_{ij}$ in the last term in the integral are positive semi-definite. Note that the entropy can only increase in the domain based on data that convects and diffuses through the boundaries, $\partial\Omega$. The sign of the entropy change from viscous dissipation is always negative.

III.C. Semi-Discrete Entropy Analysis

The semi-discrete entropy estimate is achieved by mimicking term by term the continuous estimate given in equation (III.5). As for the continuous case, the nonlinear stability (entropy stability) analysis begins by contracting the discrete entropy variables, $\mathbf{w}^\top$, with the semi-discrete version of the system (III.1) (see for instance, references[5,6]). (For clarity of presentation, but without loss of generality, the derivation is simplified to one spatial dimension. Tensor product algebra allows the results to extended directly to three-dimensions.) The resulting global equation that governs the semi-discrete decay of entropy is given in reference 5,

$$\mathbf{w}^\top \mathcal{P}\mathbf{q}_t + \mathbf{w}^\top \Delta\bar{\mathbf{f}} = \mathbf{w}^\top \Delta\bar{\mathbf{f}}^{(V)} + \mathbf{w}^\top \mathbf{g}^{(B)} + \mathbf{w}^\top \mathbf{g}^{(Int)}, \tag{III.6}$$

where

$$\mathbf{w} = \left(w(q_1)^\top, w(q_2)^\top, \ldots, w(q_N)^\top\right)^\top.$$

The source terms $\mathbf{g}^{(B)}$ and $\mathbf{g}^{(Int)}$ contain the enforcement of boundary and interface conditions, respectively. (Herein, the solution between adjoining elements or cells is allowed to be discontinuous. Therefore, interface penalties $\mathbf{g}^{(Int)}$ are needed to patch interfaces together). The entropy variables, $\mathbf{w}$, are defined at the solution points whereas the quantities with an over-bar, i.e., $\bar{\mathbf{f}}$ and $\overline{\mathbf{F}}$, are defined at the flux points (see Figure 1).

III.C.1. Entropy Consistent Inviscid Fluxes

The inviscid portion of equation (III.6) is entropy conservative if it satisfies

$$\mathbf{w}^\top \Delta\bar{\mathbf{f}} = \overline{F}(q_N) - \overline{F}(q_1) = F(q_N) - F(q_1) = \mathbf{1}^\top \Delta\overline{\mathbf{F}}. \tag{III.7}$$

[c] Using the entropy variables, the viscous fluxes in the i-direction are defined as $f_i^{(V)} = \widehat{c}_{ij}\frac{\partial w}{\partial x_j}$. The explicit form of the $\widehat{c}_{ij}$ matrices can be found in.[21,24]

A general strategy for constructing an entropy conservative flux, $\overline{f}_i^{(S)}$, that satisfies the point-wise conditions

$$(w_{i+1}-w_i)\,\overline{f}_i^{(S)} = \widetilde{\psi}_{i+1} - \widetilde{\psi}_i, \quad i = 1,2,\ldots,N-1 \quad ; \quad \widetilde{\psi}_1 = \psi_1, \quad \widetilde{\psi}_N = \psi_N \tag{III.8}$$

is presented elsewhere.[22] Herein, the flux $\overline{f}_i^{(S)}$ is based on linear combinations of q_{ij}-weighted, two-point entropy conservative fluxes $\overline{f}_S = \overline{f}_S(u_\ell, u_k)$, which satisfy the following relation:

$$(w_\ell - w_k)\,\overline{f}_S(u_\ell,u_k) = \psi_\ell - \psi_k. \tag{III.9}$$

The dyadic shuffle conditions given by equation (VII.10) are known to exist for Burgers' equation and the Euler equations.[25,28]

The following theorem summarizes the work given in reference 22, and provides the general formula for constructing $\overline{f}_i^{(S)}$ of any order from a linear combination of dyadic entropy conservative fluxes $\overline{f}_S(u_\ell,u_k)$.

Theorem 4. *A two-point high-order accurate entropy conservative flux satisfying equation* (III.8) *with formal boundary closures can be constructed as*

$$\overline{f}_i^{(S)} = \sum_{k=i+1}^{N} \sum_{\ell=1}^{i} 2\,q_{\ell k}\,\overline{f}_S(u_\ell,u_k), \quad 1 \le i \le N-1,$$

where $\overline{f}_S(u_\ell,u_k)$ is any two-point non-dissipative flux function that satisfies the entropy conservation condition given by equation (VII.10)*. The two-point high-order accurate entropy conservative flux, $\overline{f}_i^{(S)}$, satisfies an additional local entropy conservation property,*

$$\mathbf{w}^\top \mathcal{P}^{-1} \Delta \bar{\mathbf{f}}^{(S)} = \mathcal{P}^{-1} \Delta \overline{\mathbf{F}} = \frac{\partial \overline{\mathbf{F}}}{\partial x}(\mathbf{q}) + \mathcal{T}_{p+1}, \tag{III.10}$$

or equivalently,

$$w_i^\top \left(\overline{f}_i^{(S)} - \overline{f}_{i-1}^{(S)} \right) = \left(\overline{F}_i - \overline{F}_{i-1} \right), \quad 1 \le i \le N, \tag{III.11}$$

where

$$\overline{F}_i = \sum_{k=i+1}^{N} \sum_{\ell=1}^{i} q_{\ell k} \left[(w_\ell + w_k)^\top \overline{f}_S(u_\ell,u_k) - (\psi_\ell + \psi_k) \right], \quad 1 \le i \le N-1. \tag{III.12}$$

Proof. For brevity, the proof is not included herein, but is reported elsewhere.[22] □

IV. Stability on Staggered Grids: Burgers' Equation

IV.A. Data Mechanics

Define a staggered grid algorithm for building discrete differentiation operators using two sets of collocation points: $\tilde{\mathbf{x}}$ and $\mathbf{x}$ of dimension M and N, respectively. Assume that the time-dependent solution is stored at the points $\tilde{\mathbf{x}}$. Furthermore, assume that the extrema of $\mathbf{x}$ coincide with the endpoints of the domain: $\mathbf{x}_1 = x^L$, $\mathbf{x}_N = x^H$, to facilitate imposition of interface or boundary data.

Discrete differentiation of first or second order spatial terms (e.g., $\partial f/\partial x$ or $\partial f^{(V)}/\partial x$), by using the staggered grid algorithm is accomplished as follows:

- Interpolate the discrete entropy variables from $\tilde{\mathbf{x}}$ to $\mathbf{x}$.
- Build the nonlinear fluxes f and $f^{(V)}$ on the set of points $\mathbf{x}$.
- Build the interface and/or boundary penalties at the extrema of $\mathbf{x}$.
- Differentiate the fluxes on $\mathbf{x}$, and impose the penalties by using the SAT approach.
- Interpolate the discrete flux derivatives and penalties back to $\tilde{\mathbf{x}}$.

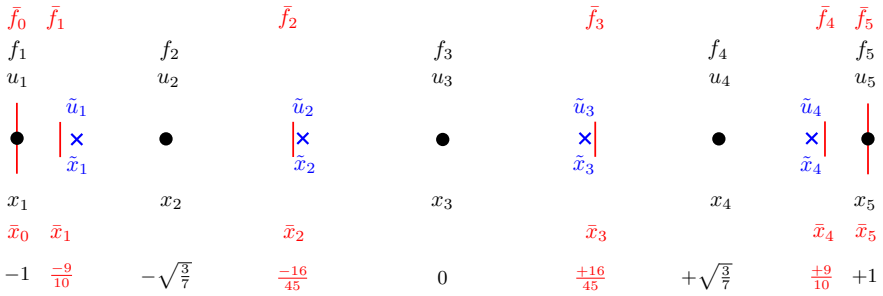

Figure 2. The one-dimensional discretization for the fourth-order accurate polynomial interpolation ($p=4$) with the staggered approach is illustrated. Solution points $\tilde{\mathbf{x}}$ are identified with $\times$ and auxiliary points $\mathbf{x}$ are identified with $\bullet$. Flux points $\bar{\mathbf{x}}$ (used to prove the entropy stability) are identified with $|$.

- Advance the solution with a time integration scheme by using the interpolated flux derivative on $\tilde{\mathbf{x}}$.

Tensor product arithmetic extends the approach directly to three spatial dimensions.[d] An SBP-SAT stability proof is now presented for the Sta-Grd-Alg. It is valid for all diagonal-norm SBP operators.

An SBP-SAT stability proof exists for the staggered grid algorithm, for all diagonal norm SBP operators. Define "tilde" variables and operators that act on the set of points: $\tilde{\mathbf{x}}$ (e.g., $\tilde{\mathbf{u}}$, $\tilde{\mathcal{P}}$ and $\tilde{\mathcal{D}}$), and the pair of interpolation operators: I_{G2LGL} and I_{LGL2G}. The I_{G2LGL} operator transfers data from $\tilde{\mathbf{x}}$ to $\mathbf{x}$, while the I_{LGL2G} transfers data from $\mathbf{x}$ to $\tilde{\mathbf{x}}$. Define the interpolated solution vector $\mathbf{u}$, and the diagonal velocity and viscosity matrices $[\sqcap]$ and $[\varepsilon]$ as

$$\mathbf{u} = I_{G2LGL}\,\tilde{\mathbf{u}} \quad ; \qquad [\sqcap] = Diag[I_{G2LGL}\tilde{\mathbf{u}}] \quad ; \qquad [\varepsilon] = Diag[I_{G2LGL}\tilde{\varepsilon}] \quad . \tag{IV.1}$$

and the boundary operator nomenclature

$$u(x_L) = \mathbf{u}|_{x=0} \quad ; \qquad (\mathcal{D}\mathbf{u})(x_L) = (\mathcal{D}\mathbf{u})|_{x=0} \quad ; \qquad \mathbf{e}(x_L) = [1,0,\cdots,0]^{\top}_{M} \quad , \tag{IV.2}$$

with similar definitions for $u(x_R)$, $(\mathcal{D}\mathbf{u})(x_R)$, and $\mathbf{e}(x_R)$.

IV.B. Stability of Burgers' Equation

An energy/entropy analysis of 1D Burgers' equation is presented before that of the compressible Navier-Stokes equations. Conventional energy estimates as well as entropy analysis exists for Burgers' equation for all diagonal norm SBP operators.[25,3,29,30] Comparison of the two approaches provides insight on how to proceed with the analysis of the compressible Navier-Stokes equations.

Consider the Burgers' equation

$$\begin{gathered} u_t + f(u)_x = [\varepsilon f^{(v)}]_x, \quad f(u) = \frac{u^2}{2}, \quad f^{(v)} = u_x, \quad x \in [x_L, x_R], \quad t \in [0,\infty), \\ \frac{u(x_L,t) + |u(x_L,t)|}{3} u(x_L,t) - \varepsilon u_x(x_L,t) - g_L(t) = 0, \\ \frac{u(x_R,t) - |u(x_R,t)|}{3} u(x_R,t) - \varepsilon u_x(x_R,t) + g_R(t) = 0, \\ u(x,0) = g_0(x) \end{gathered} \tag{IV.3}$$

with boundary conditions in (IV.3) constructed such that the semi-discrete energy only increases with respect to the imposed data and maintains the same form in the inviscid limit $\varepsilon \to 0$.

A general semi-discretization of (IV.3) suitable for energy or entropy analysis is

$$\begin{aligned} \tilde{\mathbf{u}}_t + I_{LGL2G}\,\mathcal{D}\,\hat{f}(\mathbf{u}) \;&=\; I_{LGL2G}\,\mathcal{D}\,\mathcal{E}\,\mathcal{D}\,\mathbf{u} \\ &- \left(\tfrac{u(x_L)+|u(x_L)|}{3} u(x_L) - \varepsilon(\mathcal{D}\mathbf{u})(x_L) - g(x_L)\right) I_{LGL2G}\mathcal{P}^{-1}\,\mathbf{e}(x_L) \\ &+ \left(\tfrac{u(x_R)-|u(x_R)|}{3} u(x_R) - \varepsilon(\mathcal{D}\mathbf{u})(x_R) - g(x_R)\right) I_{LGL2G}\mathcal{P}^{-1}\,\mathbf{e}(x_R) \end{aligned} \tag{IV.4}$$

[d] The Sta-Grd-Alg is valid for other grid distributions that do not support tensor product arithmetic.

with the initial data $\tilde{\mathbf{u}}(x,0) = \mathbf{f}(x)$.

The nonlinear energy stability proofs for Burgers' equation is now presented. The proof uses conventional energy analysis and a canonical alpha-flux splitting technique. It also assumes that the solution is stored at the Gauss points and is interpolated to the LGL points to achieve a statement of stability.

IV.B.1. Energy Analysis

Canonically split the quadratic term in Burgers' equation (IV.3) ($2/3$ of conservative form plus $1/3$ of chain rule form) and then apply the staggered grid algorithm to all spatial terms. The resulting semi-discrete staggered grid operator is

$$\begin{aligned} \tilde{\mathbf{u}}_t + \tfrac{1}{3}\, I_{LGL2G}\left(\mathcal{D}\left[\sqcap\right] + \left[\sqcap\right]\mathcal{D}\right)\mathbf{u} &= I_{LGL2G}\,\mathcal{D}\left[\varepsilon\right]\mathcal{D}\,\mathbf{u} \\ &- \left(\tfrac{u(x_L)+|u(x_L)|}{3}u(x_L) - \varepsilon(\mathcal{D}\mathbf{u})(x_L) - g(x_L)\right) I_{LGL2G}\,\mathcal{P}^{-1}\,\mathbf{e}(x_L) \\ &+ \left(\tfrac{u(x_R)-|u(x_R)|}{3}u(x_R) - \varepsilon(\mathcal{D}\mathbf{u})(x_R) - g(x_R)\right) I_{LGL2G}\,\mathcal{P}^{-1}\,\mathbf{e}(x_R) \end{aligned} \tag{IV.5}$$

with the initial data $\tilde{\mathbf{u}}(x,0) = \mathbf{f}(x)$.

Theorem 5. *The semi-discrete solution* $\tilde{\mathbf{u}}$ *defined in equation* (IV.5) *is bounded for all time for any diagonal norm SBP operator* $\mathcal{D}$*, provided there exist interpolation operators* I_{G2LGL} *and* I_{LGL2G} *that satisfy the constraint*

$$\tilde{\mathcal{P}}\, I_{LGL2G} = {I_{G2LGL}}^{\top}\mathcal{P} \quad ,$$

and provided the boundary data $|g(x_L)|$ *and* $|g(x_R)|$ *are bounded.*

Proof. The proof to this theorem proceeds by standard energy analysis techniques and can be found in reference 9. □

IV.B.2. Entropy Analysis

An entropy-entropy flux pair, a potential-potential flux pair, and the entropy variable, w, for Burgers' equation are[25]

$$(S,F) = \left(\frac{u^2}{2}, \frac{u^3}{3}\right) \quad ; \quad (\phi,\psi) = \left(\frac{u^2}{2}, \frac{u^3}{6}\right) \quad ; \quad u = w \quad . \tag{IV.6}$$

Note that the entropy is guaranteed convex ($S_{uu} = 1$) for all u, and that the entropy is (chosen) equivalent to the energy used in the SBP analysis.[e]

Consider the entropy analysis of equation (IV.4). Apply the staggered grid algorithm to construct the quadratic inviscid and linear viscous fluxes as well as the boundary penalties. As with the collocated approach,[5] the entropy and energy analyses of the time, viscous, and SAT terms are equivalent when using the staggered grid algorithm, while differences appear in the analysis of the quadratic flux term. In the entropy analysis the quadratic flux is discretized using a diagonal norm SBP operator: $\mathcal{D} = \mathcal{P}^{-1}Q$. The Q operator is then rearranged into telescoping form.[9] The resulting expression for the quadratic term discretized using the staggered grid algorithm is

$$\frac{1}{2}(u^2)_x \approx \mathcal{P}^{-1}\Delta\bar{\mathbf{f}}(u).$$

The resulting semi-discrete operator is

$$\begin{aligned} \tilde{\mathbf{u}}_t + I_{LGL2G}\,\mathcal{P}^{-1}\Delta\bar{\mathbf{f}}(u) &= I_{LGL2G}\,\mathcal{D}\left[\varepsilon\right]\mathcal{D}\,\mathbf{u} \\ &- \left(\tfrac{u(x_L)+|u(x_L)|}{3}u(x_L) - \varepsilon(\mathcal{D}\mathbf{u})(x_L) - g(x_L)\right) I_{LGL2G}\,\mathcal{P}^{-1}\,\mathbf{e}(x_L) \\ &+ \left(\tfrac{u(x_R)-|u(x_R)|}{3}u(x_R) - \varepsilon(\mathcal{D}\mathbf{u})(x_R) - g(x_R)\right) I_{LGL2G}\,\mathcal{P}^{-1}\,\mathbf{e}(x_R) \end{aligned} \tag{IV.7}$$

with the initial data $\mathbf{u}(x,0) = \mathbf{f}(x)$.

[e]The entropy is not unique.

What remains is to construct an entropy conserving flux $\bar{\mathbf{f}}(u) = \bar{\mathbf{f}}_i^{(S)}$. There exists an entropy conserving flux for the delta form operator: $\mathcal{P}^{-1}\Delta\bar{\mathbf{f}}(u)$, provided there exists a two-point entropy flux relation and a diagonal norm SBP operator is used for $\mathcal{D}$.

The entropy flux

$$\bar{f}_S(u_\ell, u_k) = \frac{1}{6}(u_\ell^2 + u_\ell u_k + u_k^2) \quad , \tag{IV.8}$$

which satisfies the two-point relation

$$(u_\ell - u_k)\,\bar{f}_S(u_\ell, u_k) = \frac{1}{6}(u_\ell^3 - u_k^3) \quad . \tag{IV.9}$$

The entropy conserving flux is given by

$$\bar{f}_i^{(S)} = \sum_{k=i+1}^{N}\sum_{\ell=1}^{i} 2q_{\ell k}\bar{f}_S(u_\ell, u_k) = 2\sum_{k=i+1}^{N}\sum_{\ell=1}^{i} q_{\ell k}\frac{1}{6}(u_\ell^2 + u_\ell u_k + u_k^2), \quad 1 \le i \le N-1 \quad . \tag{IV.10}$$

Contracting the quadratic term: $I_{LGL2G}\mathcal{P}^{-1}\Delta\bar{\mathbf{f}}_i^{(S)}$ in equation (IV.7) with the discrete vector $\left(\tilde{\mathcal{P}}\tilde{\mathbf{u}}\right)^\top$ yields the telescoping condition

$$\mathbf{u}^\top\Delta\bar{\mathbf{f}}^{(S)} = \mathbf{1}^\top[\sqcap]\Delta\bar{\mathbf{f}}^{(S)} = \mathbf{1}^\top\Delta\bar{\mathbf{F}} = (\bar{F}_N - \bar{F}_1) \tag{IV.11}$$

with

$$\begin{gathered}\bar{F}_i = \sum_{k=i+1}^{N}\sum_{\ell=1}^{i} q_{\ell k}\left[(u_\ell + u_k)\bar{f}_S(u_\ell, u_k) - \frac{1}{6}(u_\ell^3 + u_k^3)\right], \quad 1 \le i \le N-1, \\ \bar{F}_0 = \frac{1}{3}u_0^3, \qquad \bar{F}_N = \frac{1}{3}u_N^3.\end{gathered} \tag{IV.12}$$

Collecting all terms in the entropy analysis of Burgers' equation yields an (entropy) estimate that is identical to the energy estimate given reported in.[9]

*R*emark. The Navier-Stokes equations do not support a canonical decomposition based on the flux split technique. Thus, conventional nonlinear energy analysis is not applicable (to our knowledge). Nevertheless, the existence of a two-point entropy flux satisfying equation (III.8) enables entropy analysis to be used for all diagonal norm SBP operators.

V. The Navier-Stokes Equations in Multiple Dimensions on Staggered Grids

V.A. Staggered Grids in Two Dimensions

Extension of a 1D staggered operator to multiple dimensions can proceed in several ways. Figures 3 show two popular staggered data structures in two spatial dimensions. Both approaches store the solution at the tensor product Gauss points of order $p = 3$ (blue crosses).

The fully-staggered approach moved the data via 3D tensor product interpolations from LG (supporting a polynomial of order p) to LGL (supporting a polynomial of order $p+1$) points (black circles). The discrete operators reported in references 5, 31, 7, 6, are used on the LGL points to construct the spatial residual. The temporal updates needed on the LG points are obtained by restricting the LGL residuals back to the LG points. Extension to general curvilinear coordinates follows immediately on the LGL points.[5,7]

The semi-staggered approach moves the data via 1D interpolations from the LG to LGL points (black circles and green triangles). The inviscid terms are constructed via three 1D operations on the semi-staggered LG-LGL points. The viscous terms are most easily formed by using a fully-staggered approach. The semi-staggered operator has the advantage of not requiring corner data in the inviscid operators. However, its extension to curvilinear coordinates is not straight forward because of ambiguities in the geometric conservation law (GCL) terms. For this reason, the fully-staggered approach is used exclusively herein.

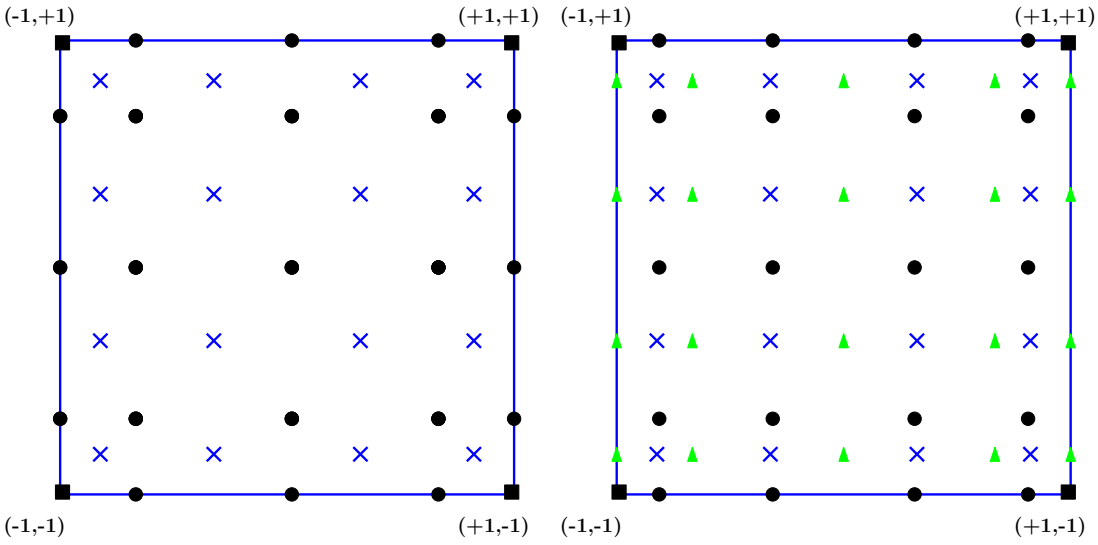

(a) Fully Staggered (b) Semi-Staggered

Figure 3. Distribution of solution and flux points for fully- and semi-staggered 2D grid algorithms.

V.B. Tensor Operators in Three Dimensions

Consider a single tensor product element and an entropy stable spatially discontinuous collocation (SSDC) discretization with $M = p+1$ LG solution points in each coordinate direction[f];[5,31,6,24] the following element-wise matrices will be used:

$$\tilde{\mathcal{P}} = \left(\tilde{\mathcal{P}}_M \otimes \tilde{\mathcal{P}}_M \otimes \tilde{\mathcal{P}}_M \otimes I_5\right),$$

$$I_{G2LGL} = \left(I_{G2LGL}\right)_{x_1x_2x_3} = \left(I_{G2LGL} \otimes I_{G2LGL} \otimes I_{G2LGL} \otimes I_5\right),$$

$$I_{LGL2G} = \left(I_{LGL2G}\right)_{x_1x_2x_3} = \left(I_{LGL2G} \otimes I_{LGL2G} \otimes I_{LGL2G} \otimes I_5\right),$$

$$\mathcal{D}_{x_1} = \left(\mathcal{D}_N \otimes I_N \otimes I_N \otimes I_5\right), \quad \cdots \quad \mathcal{D}_{x_3} = \left(I_N \otimes I_N \otimes \mathcal{D}_N \otimes I_5\right),$$

$$\mathcal{P}_{x_1} = \left(\mathcal{P}_N \otimes I_N \otimes I_N \otimes I_5\right), \quad \cdots \quad \mathcal{P}_{x_3} = \left(I_N \otimes I_N \otimes \mathcal{P}_N \otimes I_5\right), \tag{V.1}$$

$$\mathcal{P}_{x_1x_2} = \left(\mathcal{P}_N \otimes \mathcal{P}_N \otimes I_N \otimes I_5\right), \quad \cdots \quad \mathcal{P}_{x_2x_3} = \left(I_N \otimes \mathcal{P}_N \otimes \mathcal{P}_N \otimes I_5\right),$$

$$\mathcal{P} = \mathcal{P}_{x_1x_2x_3} = \left(\mathcal{P}_N \otimes \mathcal{P}_N \otimes \mathcal{P}_N \otimes I_5\right),$$

$$\mathcal{B}_{x_1} = \left(\mathcal{B}_N \otimes I_N \otimes I_N \otimes I_5\right), \quad \cdots \quad \mathcal{B}_{x_3} = \left(I_N \otimes I_N \otimes \mathcal{B}_N \otimes I_5\right),$$

$$\Delta_{x_1} = \left(\Delta_N \otimes I_N \otimes I_N \otimes I_5\right), \quad \cdots \quad \Delta_{x_3} = \left(I_N \otimes I_N \otimes \Delta_N \otimes I_5\right),$$

[f]Recall from Section **??** that with the staggered algorithm the number of LG and LGL points in 1D is denoted by M and N, respectively.

where $\tilde{\mathcal{P}}_M$ is the norm of the LG points, while $\mathcal{D}_N$, $\mathcal{P}_N$, Δ_N, and $\mathcal{B}_N$ are the 1D SBP operators[24] defined on the LGL points, and I_N is the identity matrix of dimension N. I_5 denotes the identity matrix of dimension five.[g] The subscripts in (V.1) indicate the coordinate directions to which the operators apply (e.g., $\mathcal{D}_{x_1}$ is the differentiation matrix in the x_1 direction). The symbol $\otimes$ represents the Kronecker product. When applying these operators to the scalar entropy equation in space at the LG points, a hat is used to differentiate the scalar operator from the full vector operator. For example,

$$\widehat{\tilde{\mathcal{P}}} = \left(\tilde{\mathcal{P}}_M \otimes \tilde{\mathcal{P}}_M \otimes \tilde{\mathcal{P}}_M\right) \quad ; \quad \widehat{\mathcal{P}} = \left(\mathcal{P}_M \otimes \mathcal{P}_M \otimes \mathcal{P}_M\right). \tag{V.2}$$

The vector of conservative variables of each element is ordered as

$$\tilde{\mathbf{q}} = \left(\widetilde{q}\left(\widetilde{x}_{(1)(1)(1)}\right)^\top, \widetilde{q}\left(\widetilde{x}_{(1)(1)(2)}\right)^\top, \ldots, \widetilde{q}\left(\widetilde{x}_{(M)(M)(M)}\right)^\top\right) = \left(\widetilde{q}^\top_{(1)}, \widetilde{q}^\top_{(2)}, \ldots, \widetilde{q}^\top_{(M^3)}\right), \tag{V.3}$$

where the subscripts denote the ordering of the solution points in the coordinate directions. Assume an equivalent definition and order for the entropy variables $\tilde{\mathbf{w}}$; and an analogous definition for the variables at the LGL points.[h]

The I_{G2LGL} operator transfers data from $\tilde{\mathbf{x}}$ to $\mathbf{x}$, while the I_{LGL2G} transfers data from $\mathbf{x}$ to $\tilde{\mathbf{x}}$. Define

$$\mathbf{w} = I_{G2LGL}\,\tilde{\mathbf{w}} \quad ; \qquad \widehat{c}_{ij} = I_{G2LGL}\,\tilde{c}_{ij} \quad ; \qquad [\widehat{c}_{ij}] = \mathrm{Diag}[I_{G2LGL}\,\tilde{c}_{ij}]. \tag{V.4}$$

Using these definitions and the SBP operators (V.1), system (III.1) is discretized locally on an isolated element as[24,7]

$$\frac{d\tilde{\mathbf{q}}}{dt} + I_{LGL2G}\left[\mathcal{P}^{-1}_{x_i}\Delta_{x_i}\bar{\mathbf{f}}_i - \mathcal{D}_{x_i}\bar{\mathbf{f}}^{(V)}_i\right] = I_{LGL2G}\,\mathcal{P}^{-1}_{x_i}\,\mathbf{g}^{(Int)}_i, \tag{V.5}$$

where Einstein notation is used to express the coordinate directions. The penalty interface terms $\mathbf{g}^{(Int)}_i$ with $i = 1,2,3$ are used to connect neighboring elements (see Section VI).

The entropy conservative inviscid fluxes $\bar{\mathbf{f}}_i$ of any order in equation (V.5) are computed using linear combinations of q_{ij}-weighted, two-point entropy conservative fluxes ($\overline{f}_S(u_\ell, u_k)$[22,28]) where q_{ij} denotes the coefficients of the nearly skew-symmetric matrix Q. The interpolated entropy variables $\mathbf{w} = I_{G2LGL}\,\tilde{\mathbf{w}}$ are used to build the fluxes on the LGL points. The viscous fluxes are also computed using interpolated entropy variables and the operators $\mathcal{D}_{x_i}$, $i = 1,2,3$, defined in (V.1). The viscous coefficient matrices $\widehat{c}_{ij}$ are again formed using interpolated data on the LGL points.

Remark. The interpolations from and to the LG points are carried out in computational space by using an efficient tensor-product algorithm that requires only the knowledge of the 1D I_{G2LGL} and I_{LGL2G} operators. The extension to general curvilinear coordinates follows immediately on the LGL points.[5,6]

VI. Entropy Stable Conforming Interface Coupling

Consider two cubic tensor product elements by extending equation (V.5) to two adjoining elements. Without loss of generality assume that all their faces are orthogonal to the three coordinate directions and are not boundary faces, i.e., they are not part of the boundary surface $\partial\Omega$. The resulting expressions become[24,7]

$$\frac{d\tilde{\mathbf{q}}_\ell}{dt} + I_{LGL2G\ell}\left[\mathcal{P}^{-1}_{x_i,\ell}\Delta_{x_i,\ell}\bar{\mathbf{f}}_{i,\ell} - \mathcal{D}_{x_i,\ell}[\widehat{c}_{ij,\ell}]\,\Theta_{j,\ell}\right] = I_{LGL2G\ell}\mathcal{P}^{-1}_{x_i,\ell}\,\mathbf{g}^{(Int),q}_{i,\ell}, \tag{VI.1a}$$

$$\Theta_{i,\ell} - \mathcal{D}_{x_i}\mathbf{w}_l = \mathcal{P}^{-1}_{x_i,\ell}\,\mathbf{g}^{(Int),\Theta}_{i,\ell}, \tag{VI.1b}$$

$$\frac{d\tilde{\mathbf{q}}_r}{dt} + I_{LGL2Gr}\left[\mathcal{P}^{-1}_{x_i,r}\Delta_{x_i,r}\bar{\mathbf{f}}_{i,r} - \mathcal{D}_{x_i,r}[\widehat{c}_{ij,r}]\,\Theta_{j,r}\right] = I_{LGL2Gr}\mathcal{P}^{-1}_{x_i,r}\,\mathbf{g}^{(Int),q}_{i,r}, \tag{VI.1c}$$

$$\Theta_{i,r} - \mathcal{D}_{x_i}\mathbf{w}_l = \mathcal{P}^{-1}_{x_i,r}\,\mathbf{g}^{(Int),\Theta}_{i,r}, \tag{VI.1d}$$

where the subscripts l and r denote the "left" and "right" elements. $\Theta_{i,\ell}$ and $\Theta_{i,r}$ are the vectors of the gradient of the entropy variables on the left and right elements in the i direction, whereas $\mathbf{g}^{(Int),q}_{i,(\cdot)}$ and $\mathbf{g}^{(Int),\Theta}_{i,(\cdot)}$ are the penalty interface

[g] The 3D compressible Navier-Stokes equations form a system of five nonlinear partial differential equations.

[h] With the staggered algorithm, the number of LGL points in 1D is denoted by N (see Section **??**). Thus, N^3 is the number of LGL points in a 3D tensor-product element.

terms on the conservative variable and the gradient of the entropy variable, respectively.[24] As indicated in (V.4), the matrices $[\widehat{c}_{ij}]$ are block diagonal matrices with N^3 five-by-five blocks corresponding to the viscous coefficients of each LGL point.[i] Note that (VI.1) is obtained by using $f_i^{(V)} = \widehat{c}_{ij}\, w_{x_j} = \widehat{c}_{ij}\, \Theta_j$.

The interface penalty terms are constructed as a combination of a local discontinuous Galerkin-type (LDG-type) approach and an interior penalty (IP) technique:[7]

$$\begin{aligned}\mathbf{g}_{1,l}^{(Int),q} = &\left[+\bar{\mathbf{f}}_1^{(-)} - \mathbf{f}^{ssr}(q_i^{(-)}, q_i^{(+)})\right]\mathbf{e}^{(-)} + \left[-\frac{1}{2}(1+\alpha)\left(\left[\widehat{c}_{1,j}^{(-)}\right]\Theta_j^{(-)} - \left[\widehat{c}_{1,j}^{(+)}\right]\Theta_j^{(+)}\right)\right]\mathbf{e}^{(-)} \\ &+ \left[\frac{1}{2}[L]\left(\mathbf{w}^{(-)} - \mathbf{w}^{(+)}\right)\right]\mathbf{e}^{(-)},\end{aligned} \tag{VI.2a}$$

$$\mathbf{g}_{1,l}^{(Int),\Theta} = \left[-\frac{1}{2}(1-\alpha)\left(\mathbf{w}^{(-)} - \mathbf{w}^{(+)}\right)\right]\mathbf{e}^{(-)}, \tag{VI.2b}$$

$$\begin{aligned}\mathbf{g}_{1,r}^{(Int),q} = &\left[-\bar{\mathbf{f}}_1^{(+)} + \mathbf{f}^{ssr}(q_i^{(-)}, q_i^{(+)})\right]\mathbf{e}^{(+)} + \left[+\frac{1}{2}(1-\alpha)\left(\left[\widehat{c}_{1,j}^{(+)}\right]\Theta_j^{(+)} - \left[\widehat{c}_{1,j}^{(-)}\right]\Theta_j^{(-)}\right)\right]\mathbf{e}^{(+)} \\ &+ \left[\frac{1}{2}[L]\left(\mathbf{w}^{(+)} - \mathbf{w}^{(-)}\right)\right]\mathbf{e}^{(+)},\end{aligned} \tag{VI.2c}$$

$$\mathbf{g}_{1,r}^{(Int),\Theta} = \left[+\frac{1}{2}(1+\alpha)\left(\mathbf{w}^{(+)} - \mathbf{w}^{(-)}\right)\right]\mathbf{e}^{(+)}. \tag{VI.2d}$$

The LDG penalty terms involve the coefficients $\frac{1}{2}(1\pm\alpha)$ and act only in the normal direction to the face. The IP terms involve the block diagonal parameter matrix, $[L] = \mathrm{Diag}\,[L]$, with N^3 five-by-five blocks, L, which are left unspecified for the moment.[j]

Herein, the solution between adjoining elements is allowed to be discontinuous. An inviscid interface flux that preserves the entropy consistency of the interior high-order accurate spatial operators[5] on either side of the interface $\mathbf{f}^{ssr}(q_i^{(-)}, q_i^{(+)})$ is constructed as

$$\mathbf{f}^{ssr}(q_i^{(-)}, q_i^{(+)}) = \mathbf{f}^{sr}(q_i^{(-)}, q_i^{(+)}) + \Lambda\left(w^{(+)} - w^{(-)}\right), \tag{VI.3}$$

where $\mathbf{f}^{sr}(q_i^{(-)}, q_i^{(+)})$ is the entropy *conservative* inviscid interface flux of any order.[15,5,31,24,6] Λ is a negative semi-definite interface matrix with zero or negative eigenvalues. The superscripts $(-)$ and $(+)$ denote the collocated values on the left and right side of the interface, respectively. The entropy stable flux $\mathbf{f}^{ssr}(q_i^{(-)}, q_i^{(+)})$ is more dissipative than the entropy conservative inviscid flux $\mathbf{f}^{sr}(q_i^{(-)}, q_i^{(+)})$, as can be easily verified by contracting $\mathbf{f}^{ssr}(q_i^{(-)}, q_i^{(+)})$ against the entropy variables.[5] Note that in reference 17, grid interfaces for entropy stable finite difference schemes are studied and interface fluxes similar to (VI.3) are proposed.

The stability proof for the staggered grid Navier-Stokes operator is presented elsewhere.[9,10]

VII. Entropy Stable Non-Conforming Interface Coupling

Figure 4 shows a schematic of a typical non-conforming interface commonly encountered when using p-refinement to locally enrich in portion of a larger domain. The polynomial orders of the left and right elements are $p = 2$ and $p = 3$, respectively. Both elements adopt a semi-staggered collocation operator as fully described in sections V and VI (see also figure 3(b)). Note that the interface collocation points no longer coincide on either side of the adjoining interface. Thus, conventional strategies fail to prove stability (linear or nonlinear), accuracy and conservation.

VII.A. Preliminaries

All forthcoming non-conforming derivations, without loss of generality will make several simplifying assumptions. Although two elements are considered in the derivations, the proofs naturally extend (via tensor arithmetic) to non-conforming interfaces involving an arbitrary number of elements. The elements will be denoted the "low-" and "high-"

[i] In the staggered algorithm framework, N^3 is the number of LGL points in a 3D tensor-product element.
[j] In the staggered algorithm framework, N^3 is the number of LGL points in a 3D tensor-product element.

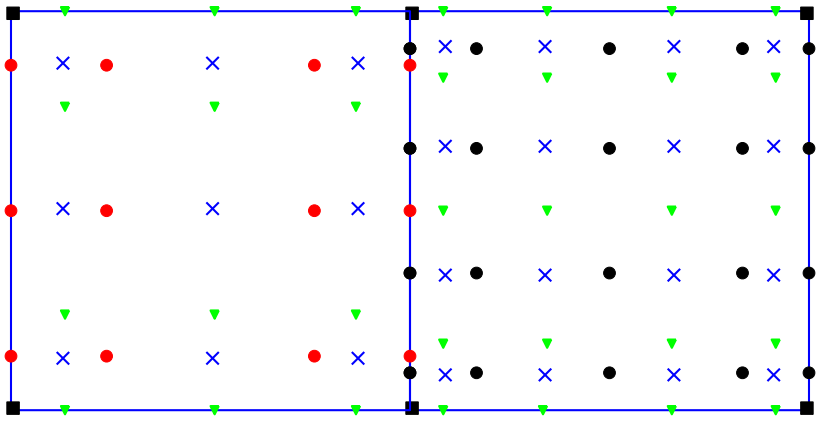

Figure 4. Non-Conforming semi-staggered 2D collocation points.

elements of polynomial orders "p_L" and "p_H", respectively. For brevity, only two spatial dimensions will be considered.

The semi-staggered approach is used exclusively in the non-conforming derivations presented herein. This design decision is motivated by the fact that the interpolated inter-facial points are LG points. The inter-element interpolation operators derived in section II.20 have the precise structural and accuracy properties needed to facilitate an entropy stable coupling.

The nonlinear compressible Euler equations will be considered in the non-conforming section. Extension to include the Navier-Stokes terms, although in principle "straight-forward", has not been attempted. The only algorithmic differences between the semi-staggered, non-conforming algorithm and the conforming algorithm presented in equation (VI.1), are the form of the penalty terms $\mathbf{g}_{i,\ell}^{(Int),q}$ and $\mathbf{g}_{i,r}^{(Int),q}$.

The derivations proceed as follows. First, a design order accurate SBP derivative operator $\mathcal{D}_x$ is constructed that couples the non-conforming interface. Next, a new generalized multi-dimensional entropy stability formulation is proposed to accommodate the nuances of the non-conforming interface. It is shown that the generalized formulation achieves $\mathcal{D}_x f = \frac{\partial f}{\partial x} + O(\delta x^{p_L})$, in multiple spatial dimensions. Finally a new entropy stability proof is formulated that is applicable for non-conforming interfaces.

VII.B. Non-Conforming SBP Operators

Tensor product formulations are sufficient to construct the base semi-staggered operators on either side of the non-conforming interface. The combined derivative operator is denoted $\bar{\mathcal{D}}_x$ and is given by

$$\bar{\mathcal{D}}_x = \mathcal{P}_x \bar{Q}_x \quad = \quad \begin{bmatrix} (\mathcal{P}_{LG}^{L\,-1} Q_{LG}^{L}) \otimes I_{LG}^{L} & 0 \\ 0 & (\mathcal{P}_{LG}^{H\,-1} Q_{LG}^{H}) \otimes I_{LG}^{H} \end{bmatrix} \quad ,$$

where the upper-left and lower-right quadrants are the p_L-order and p_H-order elements, respectively, and the terms $I_{LG}^{L,H}$ are identity matrices defined on the LG points of the p_L and p_H tensor polynomials. The "over-bars" on $\mathcal{D}_x$ and Q_x reiterate the absence of interface coupling terms via an SAT approach.

Recall that the elemental one dimensional Q operator is of the form

$$Q + Q^{\top} = \mathcal{B} = -(\mathbf{e}_1 \mathbf{e}_1{}^{\top}) + (\mathbf{e}_N \mathbf{e}_N{}^{\top}) \quad ; \quad \mathbf{e}_1 = (1,0,\cdots,0,0)^{\top} \quad ; \quad \mathbf{e}_N = (0,0,\cdots,0,1)^{\top}.$$

Thus, the left and right boundary operators for the matrix $\bar{Q}_x$, are the tensor operators

$$\mathcal{B}^L = -((\mathbf{e}_1^L \mathbf{e}_1^{L\top})_{LG}) \otimes \mathcal{P}_{LG}^L \quad ; \quad \mathcal{B}^H = +((\mathbf{e}_N^L \mathbf{e}_N^{H\top})_{LG}) \otimes \mathcal{P}_{LG}^H \quad ,$$

respectively, and are in SBP form. Indeed, all of $\bar{\mathcal{D}}_x$ satisfies the requirements of a 2D SBP operator, with the exception of the interface region. There, the tensor terms $+(\mathbf{e}_N \mathbf{e}_N{}^\top)_{LGL} \otimes \mathcal{P}_{LG}^L$ and $-(\mathbf{e}_1 \mathbf{e}_1{}^\top)_{LGL} \otimes \mathcal{P}_{LG}^H$ reside on the diagonal of the matrix $\bar{Q}_x$. What remains is to devise SAT penalty terms that couple the non-conforming interface and remove the diagonal terms of $\bar{Q}_x$. The resulting matrix Q_x is an SBP operator of the form $Q_x + Q_x^\top = \mathcal{B}_x$.

The fundamental idea of an SAT penalty operator, is to form a precise combination of interface data, such that the resulting Q matrix is skew symmetric at the interface. Achieving this by using only design order combinations of the collocated data at the interface, retains the full accuracy of the original operator.

Recall that the interface points are not collocated on the non-conforming interface. Thus, the penalty operator, Pen_x, must be constructed using interpolated interface data. Because the interface data is located on the LG points on either side of the interface, the interpolation operators I_{H2L} and I_{L2H} defined in equation (II.20), satisfy the structural conditions $I_{H2L} = \tilde{\mathcal{P}}^{-1} \mathcal{R}_{L-H}$ and $I_{L2H} = \mathcal{P}^{-1} \mathcal{R}_{L-H}^\top$. This structural constraint is a natural consequence of using the LG points on the interface, and is instrumental in achieving a skew-symmetric interface operator.

An interface penalty is presented in the following theorem that achieves the goal of skew-symmetry at the interface, while using only design order combinations of interpolated data.

Theorem 6. *A penalty coupling matrix Pen_x of the form*

$$Pen_x \quad = \quad \frac{1}{2} \begin{bmatrix} -({\mathcal{P}_{LG}^L}^{-1} \mathbf{e}_N^L \mathbf{e}_N^{L\top}) \otimes I_{LG}^L & +({\mathcal{P}_{LG}^L}^{-1} \mathbf{e}_N^L \mathbf{e}_1^{H\top}) \otimes I_{H2L} \\ -({\mathcal{P}_{LG}^H}^{-1} \mathbf{e}_1^H \mathbf{e}_N^{L\top}) \otimes I_{L2H} & +({\mathcal{P}_{LG}^H}^{-1} \mathbf{e}_1^H \mathbf{e}_1^{H\top}) \otimes I_{LG}^H \end{bmatrix}$$

provides connectivity across the non-conforming interface, and when added to the original derivative matrix $\bar{\mathcal{D}}_x$, yields a two-dimensional SBP operator, i.e.,

$$\bar{\mathcal{D}}_x + Pen_x = \mathcal{D}_x \quad ; \quad \bar{Q}_x + \mathcal{P}_x Pen_x = Q_x.$$

The resulting matrix $\mathcal{D}_x$ is of design order.

Proof. The original $\bar{Q}_x$ matrix has two diagonal block that violate the SBP structural convention. Thus, it is sufficient to only consider the interface coupling blocks. The following local block-2×2 matrix manipulation shows the addition of the interface penalty in the expression $\bar{Q}_x + \mathcal{P}_x Pen_x = Q_x$:

$$\frac{1}{2} \begin{bmatrix} \mathcal{P}_{LG}^L & 0 \\ 0 & -\mathcal{P}_{LG}^H \end{bmatrix} + \frac{1}{2} \begin{bmatrix} -\mathcal{P}_{LG}^L & \mathcal{P}_{LG}^L I_{H2L} \\ -\mathcal{P}_{LG}^H I_{L2H} & \mathcal{P}_{LG}^H \end{bmatrix} = \begin{bmatrix} 0 & \mathcal{R}_{L-H} \\ -\mathcal{R}_{L-H}^\top & 0 \end{bmatrix}.$$

The structural properties of the interpolation operators I_{H2L} and I_{L2H} defined in equation (II.20), make this manipulation possible. Thus the combined operator satisfies the following structural constraints

$$\mathcal{D}_x = \mathcal{P}_x Q_x \quad ; \quad Q_x + Q_x{}^T = \mathcal{B}_x.$$

□

Remark. Arbitrary interpolants will not in general have the structural properties required to achieve the local block-2×2 skew-symmetry in the Q_x matrix.

Remark. The interpolation operators I_{H2L} and I_{L2H} defined in equation (II.20), are exact for all 2D polynomials of order p_L. Numerical tests will be required to determine whether order reduction occurs when simulating the time-dependent Euler equations.

VII.C. Entropy Stability of Non-Conforming Interfaces

The original entropy stability proofs presented in references[21,22,9,10,5] rely on the telescoping form of the derivative operator: $f_x(\mathbf{q}) = \mathcal{P}^{-1} Q\mathbf{f} = \mathcal{P}^{-1}\Delta\bar{\mathbf{f}}$, and use a tensor product extension to achieve operators on three-dimensional curvilinear elements.

Proving nonlinear stability of a general two-dimensional SBP operator requires a different strategy. Skew-symmetry of the Q_x operator automatically gives global conservation, and tensor product arithmetic on either side of the non-conforming interface gives point-wise conservation to and from the interface. The non-conforming interface fluxes are not collocated, making the telescoping flux form $\Delta\bar{\mathbf{f}}$ ambigous at the non-conforming interface. Indeed, the operator Δ is not even uniquely defined.[k]

A generalized version of the telescoping entropy conservation is now developed. The original definitions of entropy conservation presented in equation (III.7) and theorem 8

$$\mathbf{w}^\top \Delta\bar{\mathbf{f}} = F(q_N) - F(q_1) = \mathbf{1}^\top \Delta\overline{\mathbf{F}} \quad ; \quad \overline{f}_i^{(S)} = \sum_{k=i+1}^{N} \sum_{\ell=1}^{i} 2\, q_{\ell k}\, \overline{f}_S(u_\ell, u_k), \quad 1 \le i \le N-1,$$

are now generalized to accommodate 2D SBP operators.

VII.C.1. Accuracy of Dyadic Operators

The following theorems prove that multi-dimensional high-order accurate entropy consistent discrete operators can be constructed from linear combinations of two-point entropy consistent fluxes. Although the 2D derivative operator $\mathcal{D}_x$ is used in the following proofs, the proofs generalize immediately for 3D diagonal norm SBP operators in all spatial directions.

Theorem 7. *The multi-dimensional discrete derivative operator $\mathcal{D}_x^S$,*

$$\frac{\partial f_i}{\partial x} \approx \mathcal{D}_x^S\, f|_i = \mathcal{P}_{ii}^{-1} \sum_{j=1}^{N} 2 q_{(i,j)} f_S(u_i, u_j) \quad 1 \le i \le N, \tag{VII.1}$$

achieves the design order accuracy p of the underlying SBP operator $\mathcal{D}_x = \mathcal{P}^{-1} Q_x$, provided that the fluxes $f_S(u_i, u_j)$ are non-dissipative dyadic functions derived from Tadmor's[25] integration through phase space ξ

$$f_S(u_k, u_\ell) = \int_0^1 g\left(w(u_k) + \xi\left(w(u_\ell) - w(u_k)\right)\right) \mathrm{d}\xi, \quad g(w(u)) = f(u). \tag{VII.2}$$

The coefficient $q_{(i,k)}$ corresponds to the (i,j) row and column in the SBP operator Q_x, respectively.

Proof. The proof relies upon a point-wise Taylor series analysis. By assumption, a multi-dimensional SBP operator $\mathcal{D}_x = \mathcal{P}^{-1} Q_x$ satisfies the necessary accuracy conditions given in the definition 1

$$\mathcal{D}_x \mathcal{S}_{mn} = \mathcal{S}'_{mn} \quad ; \quad \sum_{\ell=1}^{N} q_{\ell k} x_k^m y_k^n = \mathcal{P}_{(i)(i)}\, m x_i^{m-1} y_i^n \quad ; \quad \mathcal{D}F(U(x,y,z)) = \frac{\partial F}{\partial U}\frac{\partial U}{\partial x} + O((\delta x)^p) \quad , 0 \le m+n \le p$$

with $p = p_L$ the design accuracy of the operator. Note that this is a general two dimensional expansion along the path joining the two points in question. The integration in phase space proceeds as

$$\begin{aligned} f_S(u_i, u_j) &= \int_0^1 \sum_{k=0}^{\infty} \frac{1}{k!} \left.\frac{\partial^k g}{\partial w^k}\right|_{w_i} (w_j - w_i)^k \xi^k \,\mathrm{d}\xi \\ &= \sum_{k=0}^{\infty} \frac{1}{k!} \left.\frac{\partial^k g}{\partial w^k}\right|_{w_i} (w_j - w_i)^k \int_0^1 \xi^k \,\mathrm{d}\xi \\ &= \sum_{k=0}^{\infty} \frac{1}{k!} \left.\frac{\partial^k g}{\partial w^k}\right|_{w_i} (w_j - w_i)^k \frac{1}{k+1}, \end{aligned} \tag{VII.3}$$

[k] All test cases p_L and p_H performed to date, allow for a telescoping decomposition, although a general pattern has not been identified.

and simplifies to

$$f_S(u_i,u_j) = g(w_i) + \sum_{k=1}^{\infty} \frac{1}{(k+1)!} \left.\frac{\partial^k g}{\partial w^k}\right|_{w_i} (w_j - w_i)^k. \tag{VII.4}$$

Expand the terms $(w_j - w_i)^k$ using Pascal's triangle relation

$$(w_j - w_i)^k = \sum_{\ell=0}^{k} (-1)^\ell \frac{k!}{\ell!\,(k-\ell)!} w_i^\ell\, w_j^{k-\ell} \quad , \tag{VII.5}$$

and substitute expressions (VII.4) and (VII.5) back into the expression given by theorem 8, to yield

$$\mathcal{D}_x^S\, f|_i = \mathcal{P}_{ii}^{-1} \sum_{j=1}^{N} 2q_{ij} \left[g(w_i) + \sum_{k=1}^{\infty} \frac{1}{(k+1)!} \left.\frac{\partial^k g}{\partial w^k}\right|_{w_i} \left[\sum_{\ell=0}^{k} (-1)^\ell \frac{k!}{\ell!\,(k-\ell)!} w_i^\ell\, w_j^{k-\ell} \right] \right].$$

The first term vanishes because all rows of Q sum to zero and $g(w_i)$ is independent of j. Next, rearrange the sums as follows:

$$\mathcal{D}_x^S\, f|_i = \sum_{k=1}^{\infty} \frac{2}{(k+1)!} \left.\frac{\partial^k g}{\partial w^k}\right|_{w_i} \left[\sum_{\ell=0}^{k} (-1)^\ell \frac{k!}{\ell!\,(k-\ell)!} w_i^\ell \sum_{j=1}^{N} \mathcal{P}_{ii}^{-1} q_{ij} w_j^{k-\ell} \right].$$

The accuracy relationship given in (II.10) is now invoked to simplify the right-most derivative operator

$$\sum_{j=1}^{N} \mathcal{P}_{ii}^{-1} q_{ij} w_j^{k-\ell} = (k-\ell) w_i^{k-\ell-1} \left.\frac{\partial w}{\partial x}\right|_{x_i} + O((\delta x)^p),$$

which leads to the expression

$$\mathcal{D}_x^S\, f|_i = \sum_{k=1}^{\infty} \frac{2}{(k+1)!} \left.\frac{\partial^k g}{\partial w^k}\right|_{w_i} w_i^{k-1} \left.\frac{\partial w}{\partial x}\right|_{x_i} \left[\sum_{\ell=0}^{k} (-1)^\ell \frac{k!}{\ell!\,(k-\ell)!} (k-\ell) \right] + O((\delta x)^p). \tag{VII.6}$$

The Pascal triangle relationship given in equation (VII.5), when multiplied by the derivative exponent $(k-\ell)$, satisfies the relationship

$$\sum_{\ell=0}^{k} (-1)^\ell \frac{k!}{\ell!\,(k-\ell)!} (k-\ell) = \delta_{1k}, \tag{VII.7}$$

for any value of the exponent k. Substituting the value $k = 1$ into equation (VII.6) yields the desired expression

$$\mathcal{D}_x^S\, f|_i = \left.\frac{\partial g}{\partial w}\right|_{w_i} \left.\frac{\partial w}{\partial x}\right|_{x_i} + O((\delta x)^p) = f_x + O((\delta x)^p). \tag{VII.8}$$

□

VII.C.2. Entropy Stability

The discrete operator $\mathcal{D}_x^S$ given in equation (VII.1) may be expressed in matrix form as

$$\mathcal{D}_x^S f = \mathcal{P}^{-1}[Q_x f_s(u_i,u_j)]\mathbf{1} \qquad ; \qquad [Q_x f_S(u_i,u_j)] + [Q_x f_S(u_i,u_j)]^\top = [\mathcal{B}_x f_S(u_i,u_j)]. \tag{VII.9}$$

Equation (VII.9) follows immediately from the conventional definition of a SBP operator $\mathcal{D}_x = \mathcal{P}^{-1} Q_x$, and the fact that the dyadic flux $f_S(u_i,u_j)$ is symmetric with respect to the indices i, j.

Theorem 8. *The multi-dimensional discrete operator $\mathcal{D}_x^S$ given by the expression*

$$\mathcal{D}_x^S f = \mathcal{P}^{-1}[Q_x f_s]\mathbf{1}$$

is entropy conservative provided that the fluxes $f_S(u_\ell, u_k)$ are dyadic, non-dissipative functions that satisfies the entropy consistency condition

$$(w_i - w_j)\bar{f}_S(u_i, u_j) = \psi_i - \psi_j. \tag{VII.10}$$

The operator satisfies an additional local entropy consistency property,

$$2[W]\mathcal{P}^{-1}[Q_x f_S(u_i, u_j)]\mathbf{1} = 2\mathcal{P}^{-1}[Q_x F_S]\mathbf{1} = F_x + O((\delta x)^p), \tag{VII.11}$$

where

$$2\mathcal{P}^{-1}[Q_x F_S]\mathbf{1} = \mathcal{P}_{ii}^{-1}\sum_{j=1}^{N} 2q_{(i,j)}\left[\frac{(w_i + w_j)}{2} f_S(u_i, u_j) - \frac{(\psi_i + \psi_j)}{2}\right], \quad 1 \le i \le N. \tag{VII.12}$$

Proof. Using (VII.9) and the properties of SBP operators, the inner product of the entropy variables with the discrete operator $\mathcal{D}_x^S$ can be expressed as

$$\mathbf{w}^\top \mathcal{P}\mathcal{D}_x^S f = \mathbf{w}^\top 2[Q_x f_S(u_i, u_j)]\mathbf{1} = \sum_{i=1}^{N}\sum_{j=1}^{N} +q_{(i,j)} w_i f_S(u_i, u_j) - q_{(j,i)} w_i f_S(u_j, u_i) + b_{(i,j)} w_i f_S(u_i, u_j). \tag{VII.13}$$

Using the structure of $\mathcal{B}$ and recognizing that the summation indices are arbitrary, (i.e., $q_{(j,i)} w_i = q_{(i,j)} w_j$), we re-write (VII.13) as

$$\mathbf{w}^\top \mathcal{P}\mathcal{D}_x^S f = \oint_\Gamma w^\top f \bullet \vec{n}_x d\Gamma + \sum_{i=1}^{N}\sum_{j=1}^{N} q_{(i,j)}(w_i - w_j)\bar{f}_S(u_i, u_j). \tag{VII.14}$$

Any flux that satisfies (VII.10) can be used with the consistency condition $w^\top f = F + \psi$ to simplify (VII.14) to

$$\begin{aligned}\mathbf{w}^\top \mathcal{P}\mathcal{D}_x^S f = \oint_\Gamma w^\top f \bullet \vec{n}_x d\Gamma + \sum_{i=1}^{N}\sum_{j=1}^{N} q_{(i,j)}(\psi_i - \psi_j) &= \oint_\Gamma w^\top f \bullet \vec{n}_x d\Gamma + \sum_{i=1}^{N}\psi_i\sum_{j=1}^{N} q_{(i,j)} - \sum_{i=1}^{N}\sum_{j=1}^{N} q_{(i,j)}\psi_j \\ &= \oint_\Gamma (F_N + \psi_N) \bullet \vec{n}_x d\Gamma + \sum_{i=1}^{N}\sum_{j=1}^{N} q_{(i,j)}\psi_j = \oint_\Gamma F \bullet \vec{n}_x d\Gamma\,.\end{aligned}$$

The accuracy proof of the local entropy consistency property (VII.11) follows immediately from the accuracy proof of the derivative operator $\mathcal{D}_x$:

$$\mathbf{w}^\top \mathcal{P}\mathcal{D}_x^S f = w_i^\top \left(f_x(u_i) + O\left((\delta x)^d\right)\right) = F_x(u_i) + O\left((\delta x)^d\right) \quad . \tag{VII.15}$$

To show that the high-order operator given in theorem 7 satisfies the local entropy consistency property (III.11), we start by writing the derivative operator as

$$\begin{aligned}2W\mathcal{D}_x^S f = 2W\mathcal{P}^{-1}[Q_x f_s(u_i, u_j)]\mathbf{1} &= \sum_{j=1}^{N} 2\mathcal{P}_{ii}^{-1} w_i q_{(i,j)} f_S(u_i, u_j)\,;\, 1 \le i \le N \\ &= \sum_{j=1}^{N} \mathcal{P}_{ii}^{-1}(w_i + w_j) q_{(i,j)} f_S(u_i, u_j) \\ &+ \quad \mathcal{P}_{ii}^{-1}(w_i - w_j) q_{(i,j)} f_S(u_i, u_j)\,;\, 1 \le i \le N \\ &= \sum_{j=1}^{N} 2\mathcal{P}_{ii}^{-1} q_{(i,j)}\left[\frac{(w_i + w_j)}{2} f_S(u_i, u_j) + \frac{(\psi_i - \psi_j)}{2}\right].\end{aligned}$$

Adding zero

$$-\psi_i \sum_{j=1}^{N} 2q_{(i,j)} = 0$$

yields the desired result,

$$2[W]\mathcal{P}^{-1}[Q_x f_S(u_i,u_j)]\mathbf{1} = \mathcal{P}_{ii}^{-1}\sum_{j=1}^{N} 2q_{(i,j)}\left[\frac{(w_i+w_j)}{2}f_S(u_i,u_j) - \frac{(\psi_i+\psi_j)}{2}\right], \quad 1\le i\le N.$$

□

Using theorems 7 and 8, we are guaranteed that the extension of the two-point flux given in equation (VII.10), is a high-order accurate entropy consistent discretization of the conservation law.

Remark. The entropy consistency proof is satisfied for all two-point fluxes that satisfy (VII.10). The accuracy proof has only been proven for fluxes in the integral form (VII.2). We are at this point unable to show that any flux satisfying (VII.10) will be design-order accurate, so such fluxes should be validated for accuracy independent of theorem 7.

VII.D. SAT-Penalties

The two previous proofs establish entropy conservation and stability of the non-conforming interface operators. The proofs rely on the general skew-symmetry properties of the SBP operators. In practice, one implements the operators element-by-element using SAT penalties to couple the elements. Next, the previous entropy stability proofs are reformulated into a form that facilitates implementation.

Consider two tensor product elements and use equation (V.5) in the interior of the element. Assume the elements have order p_L and p_H, respectively, and that all conforming interfaces are discretized with the semi-staggered algorithm described by equation (VI.1). Without loss of generality assume that all their faces are orthogonal to the two coordinate directions and are not boundary faces, i.e., they are not part of the boundary surface $\partial\Omega$.

The resulting expressions that describe the non-conforming interface are expressed as

$$\frac{d\tilde{\mathbf{q}}^L}{dt} + {I_{LGL2G}}^L\left[(\mathcal{P}_{x_i}^H)^{-1}\bar{Q}_{LGL_i}^S\mathbf{f}_i^L\right] = {I_{LGL2G}}^L(\mathcal{P}_{x_i}^H)^{-1}\mathbf{g}_i^L, \tag{VII.16a}$$

$$\frac{d\tilde{\mathbf{q}}^H}{dt} + {I_{LGL2G}}^H\left[(\mathcal{P}_{x_i}^H)^{-1}\bar{Q}_{LGL_i}^S\mathbf{f}_i^H\right] = {I_{LGL2G}}^H(\mathcal{P}_{x_i}^H)^{-1}\mathbf{g}_i^H, \tag{VII.16b}$$

where the subscripts L and H denote the "p_L" and "p_H" order elements. and $\mathbf{g}_i^{(\cdot)}$ is the penalty interface terms on the conservative variables. The operators $\bar{Q}_{LGL_i}^S$ are entropy conservative in their interiors, but not at the adjoining non-conforming interface.

The interface penalty terms are constructed as follows:

$$\mathbf{g}_i^L = \left[+\bar{\mathbf{f}}_i^{(-)} - \mathbf{f}^{\mathbf{ssr}L}_i\right]\mathbf{e}^{(-)} \quad ; \quad \mathbf{g}_i^H = \left[+\bar{\mathbf{f}}_i^{(+)} - \mathbf{f}^{\mathbf{ssr}H}_i\right]\mathbf{e}^{(+)} \tag{VII.17}$$

with the entropy dissipative interior fluxes defined on either side of the non-conforming interface $\mathbf{f}^{\mathbf{ssr}}$ constructed as

$$\begin{aligned}
\mathbf{f}^{\mathbf{ssr}L}_i|_{x_k} &= \textstyle\sum_{j=1}^{(p_H+1)} I_{H2L(k,j)}\mathbf{f}^{\mathbf{sr}}(q_k^L,q_j^H) + \Lambda\left(w_k^L - \textstyle\sum_{j=1}^{(p_H+1)} I_{H2L(k,j)}w_j^H\right), \\
\mathbf{f}^{\mathbf{ssr}H}_i|_{x_k} &= \textstyle\sum_{j=1}^{(p_L+1)} I_{L2H(k,j)}\mathbf{f}^{\mathbf{sr}}(q_j^L,q_k^H) + \Lambda\left(w_k^H - \textstyle\sum_{j=1}^{(p_L+1)} I_{L2H(k,j)}w_j^L\right) \quad .
\end{aligned} \tag{VII.18}$$

The flux $\mathbf{f}^{\mathbf{sr}}$ is the dyadic inviscid flux.[15,5,31,24,6] The first sum in equation (VII.18) accounts for the off element entropy fluxes required for entropy stability when using $\bar{Q}_x$. The second sum provides a Lax-Friedrichs interface dissipation.

The entropy stable flux $\mathbf{f}^{\mathbf{ssr}}$ is more dissipative than the entropy conservative inviscid flux $\mathbf{f}^{\mathbf{sr}}$, provided that the matrix Λ is negative semi-definite (NSD) (i.e., zero or negative eigenvalues). This is verified by contracting ${\mathbf{f}^{\mathbf{ssr}}}_i$ against the entropy variables w_i on either side of the non-conforming interface and summing both contributions as follows

$$\Upsilon^{(I)} = {\mathbf{w}^L}^\top\mathcal{P}_{LG}^L\Lambda(\mathbf{w}^L - I_{H2L}\mathbf{w}^H) + {\mathbf{w}^H}^\top\mathcal{P}_{LG}^H\Lambda(\mathbf{w}^H - I_{L2H}\mathbf{w}^L) = (\mathbf{w}^H - I_{L2H}\mathbf{w}^L)^\top\mathcal{P}_{LG}^H\Lambda(\mathbf{w}^H - I_{L2H}\mathbf{w}^L) \quad . \tag{VII.19}$$

The sum of terms at the non-conforming interface $\Upsilon^{(I)}$ is NSD provided that Λ is NSD. The matrix identity $I_{H2L}I_{L2H} = I^L$ is used to simplify the equation (VII.19).

*R*emark. The entropy conservative fluxes are globally conservative in an integral sense, but not point-wise on the non-conforming interface.

VIII. Results: Accuracy and Robustness

VIII.A. Fully Staggered Approach and Conforming Interfaces

VIII.A.1. Viscous Shock

The first test case considered in this section is the propagation of a viscous shock for which an exact time-dependent solution is known. The compressible Navier-Stokes equations support an exact solution for the viscous shock profile, under the assumption that the Prandtl number is $Pr = \frac{3}{4}$. Mass and total enthalpy are constant across a shock. Furthermore, if $Pr = \frac{3}{4}$ then the momentum and energy equations are redundant. The single momentum equation across the shock is given by

$$\begin{gathered} \alpha v \frac{\partial v}{\partial x_1} - (v-1)(v-v_f) = 0 \quad ; \quad -\infty \leq x_1 \leq \infty \quad , \quad t \geq 0; \\ v = \frac{u_1}{u_{1,left}} \, ; \, v_f = \frac{u_{1,right}}{u_{1,left}} \, ; \, \alpha = \frac{\gamma - 1}{2\gamma} \frac{\mu}{Pr\dot{m}}, \end{gathered} \tag{VIII.1}$$

where $\dot{m}$ is the constant mass flow across the shock. An exact solution is obtained by solving the momentum equation (**??**) for the velocity profile, v:

$$x_1 = \tfrac{1}{2}\alpha \left(Log\left|(v-1)(v-v_f)\right| + \tfrac{1+v_f}{1-v_f} Log\left|\tfrac{v-1}{v-v_f}\right| \right). \tag{VIII.2}$$

A moving shock is recovered by applying a uniform translation to the solution. A full derivation of this solution appears in the thesis of Fisher.[21] In this study, the values $U_\infty = M_\infty c_\infty$, $M_\infty = 2.5$, $Re_\infty = 10$, and $\gamma = 1.4$ are used. The viscous shock, which at $t = 0$ is located at the center of the computational domain, is propagated in the direction parallel to the horizontal axis. The domain is described by

$$x_1 \in (-10, 10), \quad x_2 \in (-10, 10), \quad x_3 \in (-1, 1), \quad t \geq 0.$$

The boundary conditions on the faces perpendicular to the horizontal axis are prescribed by penalizing the numerical solution against the exact solution; periodic boundary conditions are used on the remaining four boundary faces of the computational domain. This is an excellent test problem for verifying the accuracy and functionality of the inviscid and viscous components of a compressible Navier-Stokes solver.

Different grid resolutions are examined, and the viscous shock is halfway out of the domain when the error measure is evaluated. The goal of this study is to investigate if the proposed numerical schemes are effectively $p_G + 1$-order accurate for more realistic meshes (p_G is the order of the polynomial built by using the LG points). In order to perform the grid convergence study, we construct each grid by repeating N-th times in each direction the "grid kernel" shown in Figure 5. Tables 1, 2, and 3 show the convergence study for a sequence of maximum six nested grids, for $p_G = 1, 2, 5$ and $p_{LGL} = 2, 3, 6$. The number of "grid kernel" in each coordinate direction is indicated in the first column of these tables. For the fully staggered algorithm, the L^2 norm of the error decay asymptotes towards the designed rate in each case (i.e., second order, third order, and fifth order, respectively). The conventional path[5,6] converges instead to p. Furthermore, we observe that the fully staggered approach is more accurate than the conventional algorithm for the same grid resolution.

Table 1. Error convergence is shown for the fully staggered $p_G = 1$, $p_{LGL} = 2$ and the conventional[5,6] $p_{LGL} = 1$ algorithms for the viscous shock on non-uniform grids.

	Fully staggered, $p_G = 1$, $p_{LGL} = 2$				Conventional, $p_{LGL} = 1$			
Resolution	L^2 error	L^2 rate	L^∞ error	L^∞ rate	L^2 error	L^2 rate	L^∞ error	L^∞ rate
$2 \times 2 \times 2$	1.89e-02	-	1.43e-01	-	5.07e-02	-	2.56e-01	-
$4 \times 4 \times 2$	7.85e-03	1.27	6.85e-02	1.06	2.57e-02	0.98	2.05e-01	0.32
$8 \times 8 \times 2$	2.45e-03	1.68	3.08e-02	1.15	1.16e-02	1.15	1.04e-01	0.98
$16 \times 16 \times 2$	6.46e-04	1.92	8.35e-03	1.88	6.18e-03	0.91	7.80e-02	0.42
$32 \times 32 \times 2$	1.58e-04	2.03	2.15e-03	1.96	3.04e-03	1.02	4.12e-02	0.92
$64 \times 64 \times 2$	4.04e-05	1.97	6.39e-04	1.75	1.92e-03	0.67	2.77e-02	0.57

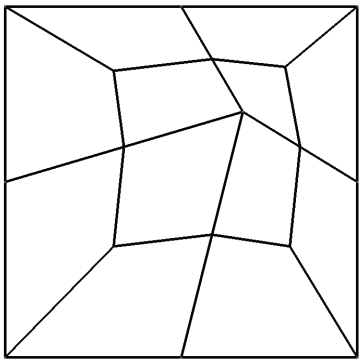

Figure 5. "Grid kernel" used to construct a sequence of nested grids for the 3D viscous shock test case.

Table 2. Error convergence is shown for the fully staggered $p_G = 2$, $p_{LGL} = 3$ and the conventional[5,6] $p_{LGL} = 2$ algorithms for the viscous shock on non-uniform grids.

	Fully staggered, $p_G = 2$, $p_{LGL} = 3$				Conventional, $p_{LGL} = 2$			
Resolution	L^2 error	L^2 rate	L^∞ error	L^∞ rate	L^2 error	L^2 rate	L^∞ error	L^∞ rate
$2 \times 2 \times 2$	5.23e-03	-	4.10e-02	-	1.28e-02	-	1.44e-01	-
$4 \times 4 \times 2$	1.03e-03	2.34	1.51e-02	1.44	4.67e-03	1.46	9.41e-02	0.62
$8 \times 8 \times 2$	1.54e-04	2.74	2.67e-03	2.49	1.23e-03	1.92	3.53e-02	1.41
$16 \times 16 \times 2$	2.34e-05	2.72	5.03e-04	2.41	2.02e-04	2.61	5.88e-03	2.59
$32 \times 32 \times 2$	3.74e-06	2.65	8.29e-05	2.60	3.63e-05	2.48	7.34e-04	3.00
$64 \times 64 \times 2$	5.30e-07	2.82	1.25e-05	2.73	8.31e-06	2.13	1.37e-04	2.42

Table 3. Error convergence is shown for the fully staggered $p_G = 5$, $p_{LGL} = 6$ and the conventional[5,6] $p_{LGL} = 5$ algorithms for the viscous shock on non-uniform grids.

	Fully staggered, $p_G = 5$, $p_{LGL} = 6$				Conventional, $p_{LGL} = 5$			
Resolution	L^2 error	L^2 rate	L^∞ error	L^∞ rate	L^2 error	L^2 rate	L^∞ error	L^∞ rate
$2 \times 2 \times 2$	2.28e-04	-	3.77e-03	-	6.79e-04	-	9.36e-03	-
$4 \times 4 \times 2$	8.23e-06	4.79	2.03e-04	4.22	5.46e-05	3.64	3.18e-03	1.56
$8 \times 8 \times 2$	2.25e-07	5.19	1.05e-05	4.26	5.13e-07	6.73	2.74e-05	6.86
$16 \times 16 \times 2$	4.02e-09	5.81	2.32e-07	5.51	1.67e-08	4.94	1.17e-06	4.55
$32 \times 32 \times 2$	6.37e-11	5.98	5.05e-09	5.52	3.52e-10	5.57	3.10e-08	5.24

VIII.A.2. Taylor-Green Vortex

The Taylor-Green vortex test case is used as a model problem to study the stability and accuracy of the provable entropy stable semi-discretization described in the previous sections. This benchmark flow problem involves only periodic boundary conditions and it is solved within a cubic domain which spans $[-\pi L, +\pi L]$ in each coordinate direction. Starting from an analytical solution characterized by a set of vortices, successive nonlinear scale interactions yield the vortices breakdown from an anisotropic laminar phase to a fully isotropic decaying turbulence. Therefore, the range of physical spatial scales increases with time up to $t \approx 9$ where the maximum spectrum of scales is reached.

Because our framework solves the compressible Navier-Stokes equations, we choose a Mach number of $M = 0.08$ which leads to a flowfield which is essentially incompressible. This allows for a fair comparison with some of the incompressible simulations reported in literature. In this abstract two Reynolds numbers are considered: $Re = 800$ and $Re = 1600$. The Prandtl number is set to $Pr = 0.72$.

$Re = 800$

In this section we report the results for $Re = 800$ on a uniform Cartesian grid with four hexahedron in each coordinate direction. Therefore, the total number of element in the grid is $N_{hexa} = 4^3 = 64$. We compute the numerical solution with the tenth- ($p_G = 9$, $p_{LGL} = 10$), sixteenth- ($p_G = 15$, $p_{LGL} = 16$), and seventeenth-order ($p_G = 16$, $p_{LGL} = 17$) accurate fully staggered algorithms. The numerical solutions presented herein are compared with the direct numerical simulation (DNS) of Brachet et al.[32] Figure 6 shows the kinetic energy dissipation rate of our computations and the reference data. It can be clearly seen that the computation with a formally seventeenth-order accurate scheme compares very well with the DNS results, even on this very coarse grid.

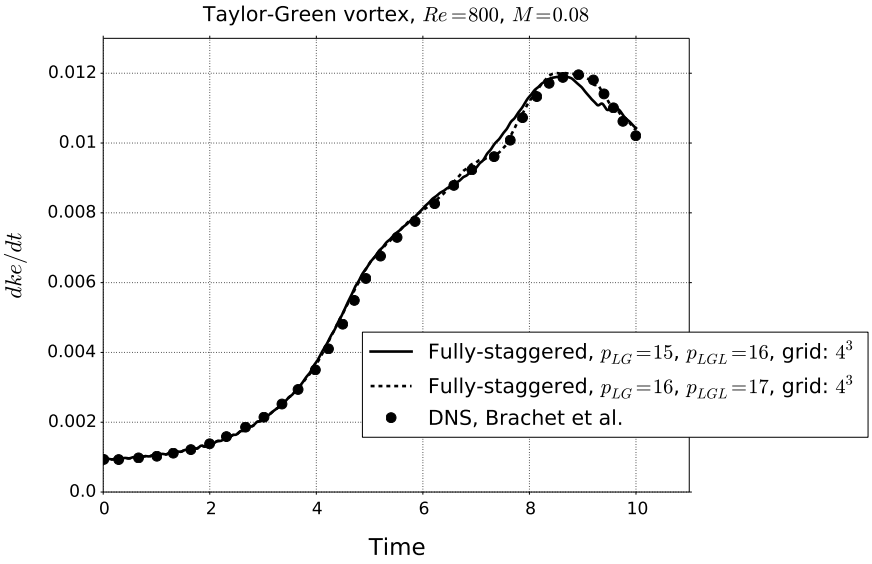

Figure 6. Evolution of the time derivative of the kinetic energy for the Taylor-Green vortex at $Re = 800$, $M = 0.08$; fully-staggered SSDC algorithm.

$Re = 1,600$

The goal of this section is to demonstrate that mathematically rigorously designed schemes do not require any stabilization technique for successful computations of under-resolved turbulent flows. The simulation is run using a fully unstructured grid which contains in total 42 hexahedrons. The distribution of the elements in the 2D plane is shown in Figure 7.

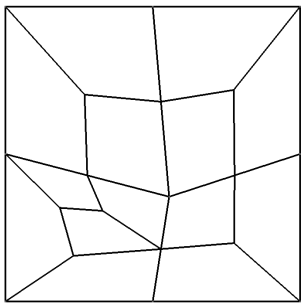

Figure 7. Plane distribution of the elements used for the Taylor-Green vortex at $Re = 1600$, $M = 0.08$.

Figure 8 shows the kinetic energy dissipation rate of our computations and the reference data of Carton de Wiart et al.[33] The grid is too coarse to accurately resolve the flow field, however, the computation with a formally seventeenth-order accurate scheme is stable through all the simulation. This is a feat unattainable with alternative approaches based on high-order accurate linear stable schemes.

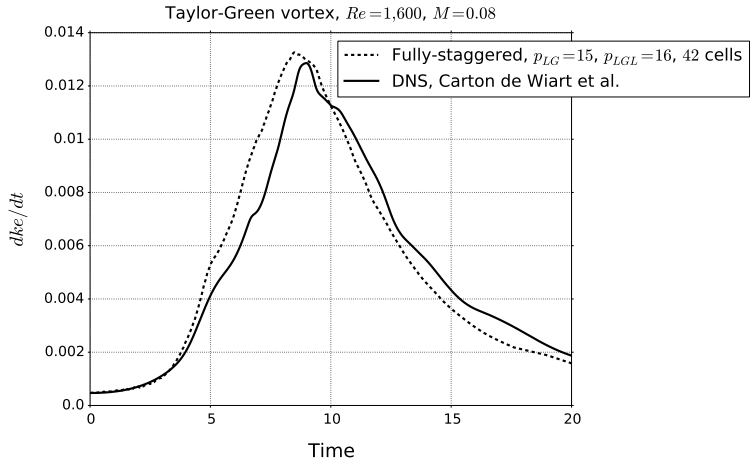

Figure 8. Evolution of the time derivative of the kinetic energy for the Taylor-Green vortex at $Re = 1600$, $M = 0.08$; staggered SSDC algorithm.

VIII.B. Semi Staggered Approach: Conforming and Non-conforming Interfaces

The semi-staggered algorithm with non-conforming interfaces is currently being implemented in three spatial dimensions. In the interim, a consistency check of the entropy fluxes is provided. Theorem 7 proves that the entropy fluxes constructed from the summation of dyadic two-point entropy fluxes retains the full accuracy of the multi-dimensional $\mathcal{D}_x$ operator, provided that the dyadic flux is derived from Tadmor's[25] integration through phase space ξ given by equation VII.2. Herein, the dyadic fluxes are calculated base on the work of Ismail and Roe,[28] which has not been shown to be of the form of equation VII.2. Thus, it is necessary to establish that order reduction is not observed when using the two-dimensional $\mathcal{D}_x^S$ operator.

Table 5 provides a convergence study using the Euler vortex exact solution, and an exact expression for $\bigtriangledown \bullet f$ based on an Euler vortex initial condition. The discrete divergence of the fluxes is used to establish the accuracy of the entropy conservative operator. Full design accuracy is expected to be order p for a polynomial of order p. The original solution is a polynomial of order p while the flux projected onto the semi-staggered grid is of order $p+1$, which when differentiated should yield order p. The results indicate that for even order polynomials full design order is achieved, while for odd order polynomials the order reduces by one.

Two types of comparisons are reported. The first reports the accuracy of the conforming interfaces. (This result should be of design order). The second reports the accuracy of the non-conforming interfaces (which should be of order p_L). The order reduction for odd order polynomials could be attributed to the absence of lifting operators in the present investigation. Nevertheless, it is encouraging that all fluxes converge at equivalent rates, whether they are entropy fluxes, or conventional fluxes constructed as in nodal DG.

IX. Conclusions

A summation-by-parts, simultaneous-approximation-term (SBP-SAT) framework is used to develop a generalized entropy stable spectral element formulation that includes a broader selection of collocation points and non-conforming interface coupling. A necessary condition for an entropy-stable, staggered operator is a restriction/prolongation interpolation pair that satisfies a precise Galerkin constraint (see equation (II.18)). This constraint is automatically satisfied when interpolating between the LG and LGL points, provided the polynomial order of the LGL points exceeds that of the LG points (as well as other less desirable combinations).

Entropy analysis is used on the 1D viscous Burgers' equation to prove the nonlinearly stability of the fully staggered operators for arbitrary order, diagonal-norm SBP operators. Next, the entropy analysis techniques presented in references 5, 6 are used to develop an entropy conservative, staggered grid, spectral collocation operator for the 3D compressible Navier-Stokes equation. Entropy conservative/stable inviscid interface operators are then developed for the staggered formulation. The viscous interface coupling is based on an LDG/IP approach analogous to the cou-

Table 4. Error convergence is shown for the semi staggered algorithm with conforming interface for $p_L = 4,5,6$, $p_H = 4,5,6$; Euler vortex propagation on uniform grids.

	$p_L = 4$, $p_H = 4$		$p_L = 5$, $p_H = 5$		$p_L = 6$, $p_H = 6$	
Resolution	L^2 error	L^2 rate	L^2 error	L^2 rate	L^2 error	L^2 rate
11	7.22E-003	-4.00	8.65E-004	-2.32	2.68E-004	-11.57
12	5.22E-003	-3.73	6.59E-004	-3.13	2.15E-004	-2.55
13	3.83E-003	-3.86	5.14E-004	-3.09	1.36E-004	-5.71
14	2.87E-003	-3.88	4.03E-004	-3.28	1.00E-004	-4.13
15	2.19E-003	-3.90	3.20E-004	-3.36	6.44E-005	-6.40
16	1.70E-003	-3.93	2.56E-004	-3.45	4.54E-005	-5.40
17	1.34E-003	-3.94	2.07E-004	-3.51	3.17E-005	-5.92
18	1.07E-003	-3.95	1.69E-004	-3.57	2.28E-005	-5.75
19	8.64E-004	-3.96	1.39E-004	-3.61	1.67E-005	-5.85
20	7.05E-004	-3.97	1.11E-004	-3.70	1.23E-005	-5.85
21	5.81E-004	-3.97	9.60E-005	-3.70	9.26E-006	-5.87
22	4.83E-004	-3.98	8.05E-005	-3.78	7.03E-006	-5.89

Table 5. Error convergence is shown for the semi staggered algorithm with non-conforming interface for $p_L = 4,5,6$, $p_H = 5,6,7$; Euler vortex propagation on uniform grids.

	$p_L = 4$, $p_H = 5$		$p_L = 5$, $p_H = 6$		$p_L = 6$, $p_H = 7$	
Resolution	L^2 error	L^2 rate	L^2 error	L^2 rate	L^2 error	L^2 rate
11	9.26E-004	-2.46	2.71E-004	-11.46	2.19E-005	2.22
12	7.04E-004	-3.15	2.60E-004	-0.51	1.10E-005	-7.89
13	5.48E-004	-3.12	1.38E-004	-7.92	9.83E-006	-1.41
14	4.29E-004	-3.29	1.01E-004	-4.13	6.33E-006	-5.94
15	3.40E-004	-3.37	6.56E-005	-6.32	4.82E-006	-3.96
16	2.73E-004	-3.44	4.65E-005	-5.33	3.44E-006	-5.23
17	2.20E-004	-3.50	3.27E-005	-5.82	2.55E-006	-4.88
18	1.80E-004	-3.55	2.37E-005	-5.63	1.90E-006	-5.21
19	1.48E-004	-3.60	1.74E-005	-5.70	1.43E-006	-5.22
20	1.22E-004	-3.78	1.30E-005	-5.68	1.08e-006	-5.48

pling operators presented in references 5, 6. The resulting spectral collocation operators are design order accurate for arbitrary order, conservative on the LGL points, and satisfy the additional secondary constraint of entropy stability. Extension to curvilinear meshes and entropy stable solid wall BCs[24,7] follow immediately.

Extensive numerical tests for the 3D Euler and compressible Navier-Stokes equations reported herein and in reference 9 reveal that the new staggered grid entropy stable algorithms are significantly more accurate than the collocated Legendre-Gauss-Lobatto operators of equivalent polynomial order, that are presented in references.[5,6] They are however, more costly to implement.[9]

The newly developed staggered grid entropy stable algorithm are next extended to include a non-conforming interface capability. Entropy conservative/stable *p*-adaptive refinement mechanics are developed for the nonlinear compressible Euler equations on hexahedral elements. A significant generalization of the existing entropy stability mechanics is required to accommodate fully multi-dimensional summation-by-parts (SBP) operators. This generalized entropy machinery will facilitate the analysis of other element types, including the closely related scenario of *h*-refinement.

Successful completion of these two objectives, brings the entropy stable spectral collocation framework closer to the maturity of conventional DG-FEM, but with the rigor of provably non-linearly stable semi-discrete operators.

Acknowledgments

Special thanks are extended to Dr. Mujeeb R. Malik for funding this work as part of the "Revolutionary Computational Aerosciences" project.

References

[1]Atkins, H. L. and Shu, C.-W., "Quadrature-free implementation of discontinuous Galerkin method for hyperbolic equations," *AIAA Journal*, Vol. 36, No. 5, 1998, pp. 775–782.

[2]Gassner, G. J., "A kinetic energy preserving nodal discontinuous Galerkin spectral element method," *International Journal for Numerical Methods in Fluids*, Vol. 76, No. 1, 2014, pp. 28–50.

[3]Hesthaven, J. S. and Warburton, T., *Nodal discontinuous Galerkin methods: Algorithms, analysis, and applications*, Texts in Applied Mathematics, Springer, 2008.

[4]Kopriva, D. A. and Gassner, G. J., "On the quadrature and weak form choices in collocation type discontinuous Galerkin spectral element methods," *Journal of Scientific Computing*, Vol. 44, No. 2, 2010, pp. 136–155.

[5]Carpenter, M. H., Fisher, T. C., Nielsen, E. J., and Frankel, S. H., "Entropy stable spectral collocation schemes for the Navier–Stokes equations: Discontinuous interfaces," *SIAM Journal on Scientific Computing*, Vol. 36, No. 5, 2014, pp. B835–B867.

[6]Parsani, M., Carpenter, M. H., and Nielsen, E. J., "Entropy stable wall boundary conditions for the three-dimensional compressible Navier–Stokes equations," *Journal of Computational Physics*, Vol. 292, 2015, pp. 88–113.

[7]Parsani, M., Carpenter, M. H., and Nielsen, E. J., "Entropy stable discontinuous interfaces coupling for the three-dimensional compressible Navier–Stokes equations," *Journal of Computational Physics*, Vol. 290, 2015, pp. 132–138.

[8]Lax, P. and Wendroff, B., "Systems of conservation laws," *Communications on Pure and Applied Mathematics*, Vol. 13, No. 2, 1960, pp. 217–237.

[9]Carpenter, M. H., Parsani, M., Fisher, T. C., and Nielsen, E. J., "Entropy stable staggered grid spectral collocation for the Burgers' and compressible Navier–Stokes equations," Tech. Rep. NASATM 1???, 2015.

[10]Parsani, M., Carpenter, M. H., Fisher, T. C., and Nielsen, E. J., "Entropy Stable Staggered Grid Spectral Collocation for the Compressible Navier-Stokes Equations," *SIAM Journal on Scientific Computing*, Submitted, November 2015.

[11]Kopriva, D. A. and Kolias, J. H., "A conservative staggered-grid Chebyshev multidomain method for compressible flows," *Journal of Computational Physics*, Vol. 125, No. 1, 1996, pp. 244–261.

[12]Liu, Y., Vinokur, M., and Wang, Z. J., "Spectral difference method for unstructured grids I: Basic formulation," *Journal of Computational Physics*, Vol. 216, No. 2, 2006, pp. 780–801.

[13]Huynh, H. T., "A flux reconstruction approach to high-order schemes including discontinuous Galerkin methods," *18th AIAA Computational Fluid Dynamics Conference*, AIAA 2007-4079, 2007.

[14]Vincent, P. E., Castonguay, P., and Jameson, A., "A new class of high-order energy stable flux reconstruction schemes," *Journal of Scientific Computing*, Vol. 47, No. 1, 2011, pp. 50–72.

[15]Fisher, T. C. and Carpenter, M. H., "High-order entropy stable finite difference schemes for nonlinear conservation laws: Finite domains," *Journal of Computational Physics*, Vol. 252, 2013, pp. 518–557.

[16]Svärd, M. and Mishra, S., "Entropy stable schemes for initial-boundary-value conservation laws," *Zeitschrift für Angewandte Mathematik und Physik*, Vol. 63, No. 6, 2012, pp. 985–1003.

[17]Svärd, M. and Özcan, H., "Entropy-stable schemes for the Euler equations with far-field and wall boundary conditions," *Journal of Scientific Computing*, Vol. 58, No. 1, 2014, pp. 61–89.

[18]Fisher, T. C., Carpenter, M. H., Nordström, J., Yamaleev, N. K., and Swanson, R. C., "Discretely conservative finite-difference formulations for nonlinear conservation laws in split form: Theory and boundary conditions," Tech. Rep. NASA TM 2011-217307, 2011.

[19]Hicken, J. E., Fernández, D. C. D. R., and Zingg, D. W., "Multi-Dimensional Summation-By-Parts Operators: General thoery and Application to Simplex Elements," *arXiv:1505.03125v3 [math.NA] 4 Sept 2015*.

[20]Carpenter, M. H. and Gottlieb, D., "Spectral methods on arbitrary grids," *Journal of Computational Physics*, Vol. 129, 1996, pp. 74–86.

[21]Fisher, T. C., *High-order L^2 stable multi-domain finite difference method for compressible flows*, Ph.D. thesis, Purdue University, 2012.

[22]Fisher, T. C., Carpenter, M. H., Nordström, J., Yamaleev, N. K., and Swanson, R. C., "Discretely conservative finite-difference formulations for nonlinear conservation laws in split form: Theory and boundary conditions," *Journal of Computational Physics*, Vol. 234, 2013, pp. 353–375.

[23]Dafermos, C. M., *Hyperbolic conservation laws in continuum physics*, Springer-Verlag, Berlin, 2010.

[24]Parsani, M., Carpenter, M. H., and Nielsen, E. J., "Entropy stable wall boundary conditions for the compressible Navier–Stokes equations," Tech. Rep. NASA TM 218282, 2014.

[25]Tadmor, E., "Entropy stability theory for difference approximations of nonlinear conservation laws and related time-dependent problems," *Acta Numerica*, Vol. 12, 2003, pp. 451–512.

[26]Tadmor, E. . and Zhong, W., "Entropy stable approximations of the Navier–Stokes equations with no artificial numerical viscosity," *Journal of Hyperbolic Differential Equations*, Vol. 3, No. 3, 2006, pp. 529–559.

[27]Merriam, M. L., "An entropy-based approach to nonlinear stability," Tech. Rep. NASA TM 101086, 1989.

[28]Ismail, F. and Roe, P. L., "Affordable, entropy-consistent Euler flux functions II: Entropy production at shocks," *Journal of Computational Physics*, Vol. 228, 2009, pp. 5410–5436.

[29]Fisher, T. C. and Carpenter, M. H., "High-order entropy stable finite difference schemes for nonlinear conservation laws: Finite domains," Tech. Rep. NASA TM-217971, 2013.

[30]Carpenter, M. H. and Fisher, T. C., "High-order entropy stable formulations for computational fluid dynamics," *21st AIAA Computational Fluid Dynamics Conference*, AIAA 2013-2868, 2013.

[31]Carpenter, M. H. and Fisher, T. C., "Entropy stable spectral collocation schemes for the Navier-Stokes equations: Discontinuous interfaces," Tech. Rep. NASA TM 218039, 2013.

[32]Brachet, M. E., Meiron, D., Orszag, S., Nickel, B., Morf, R., and Frisch, U., "The Taylor–Green vortex and fully developed turbulence," *Journal of Statistical Physics*, Vol. 34, No. 5-6, 1984, pp. 1049–1063.

[33]de Wiart, C., Hillewaert, K., Duponcheel, M., and Winckelmans, G., "Assessment of a discontinuous Galerkin method for the simulation of vortical flows at high Reynolds number," *International Journal for Numerical Methods in Fluids*, Vol. 74, No. 7, 2014, pp. 469–493.